Dieses Dokument ist eine Zweitveröffentlichung (Postprint)

This is a self-archiving document (accepted version)

Claudia Dittfeld, Cindy Welzel, Ulla König et al.

Hemocompatibility tuning of an innovative glutaraldehyde-free preparation strategy using riboflavin/UV crosslinking and electron irradiation of bovine pericardium for cardiac substitutes

Erstveröffentlichung in / First published in:

Biomaterials advances. 2023. 147. Elsevier. ISSN: 2772-9508.

DOI: https://doi.org/10.1016/j.bioadv.2023.213328

Diese Version ist verfügbar / This version is available on:

https://nbn-resolving.org/urn:nbn:de:bsz:14-qucosa2-919487

Dieses Werk ist lizenziert unter einer Creative Commons Namensnennung - Nicht kommerziell - Keine Bearbeitungen 4.0 International Lizenz.
This work is licensed under a Creative Commons Attribution-NonCommercial-NoDerivatives 4.0 International License.

SLUB Wir führen Wissen.

TECHNISCHE UNIVERSITÄT DRESDEN

QUCOSA Quality Content of Saxony

Final edited version was published in Biomaterials advances. 2023. 147. Elsevier. ISSN: 2772-9508..
https://doi.org/10.1016/j.bioadv.2023.213328

Hemocompatibility tuning of an innovative glutaraldehyde-free preparation strategy using riboflavin/UV crosslinking and electron irradiation of bovine pericardium for cardiac substitutes

Claudia Dittfeld [a,*], Cindy Welzel [a], Ulla König [c], Anett Jannasch [a], Konstantin Alexiou [a], Ekaterina Blum [c], Saskia Bronder [c], Claudia Sperling [b], Manfred F. Maitz [b,1], Sems-Malte Tugtekin [a,1]

[a] *Department of Cardiac Surgery, Carl Gustav Carus Faculty of Medicine, Technische Universität Dresden, Heart Centre Dresden, Germany*
[b] *Leibniz-Institut für Polymerforschung Dresden e.V., Institute Biofunctional Polymer Materials, Dresden, Germany*
[c] *Fraunhofer Institute for Organic Electronics, Electron Beam and Plasma Technology FEP, Dresden, Germany*

ARTICLE INFO

Keywords:
Glutaraldehyde-free pericardium preparation
Riboflavin/UV crosslinking
Electron irradiation
α-Gal
Hemocompatibility
Coagulation
Inflammation
Immune reaction

ABSTRACT

Hemocompatibility tuning was adopted to explore and refine an innovative, GA-free preparation strategy combining decellularization, riboflavin/UV crosslinking, and low-energy electron irradiation (SULEEI) procedure. A SULEEI-protocol was established to avoid GA-dependent deterioration that results in insufficient long-term aortic valve bioprosthesis durability. Final SULEEI-pericardium, intermediate steps and GA-fixed reference pericardium were exposed in vitro to fresh human whole blood to elucidate effects of preparation parameters on coagulation and inflammation activation and tissue histology. The riboflavin/UV crosslinking step showed to be less efficient in inactivating extracellular matrix (ECM) protein activity than the GA fixation, leading to tissue-factor mediated blood clotting. Intensifying the riboflavin/UV crosslinking with elevated riboflavin concentration and dextran caused an enhanced activation of the complement system. Yet activation processes induced by the previous protocol steps were quenched with the final electron beam treatment step. An optimized SULEEI protocol was developed using an intense and extended, trypsin-containing decellularization step to inactivate tissue factor and a dextran-free, low riboflavin, high UV crosslinking step. The innovative and improved GA-free SULEEI-preparation protocol results in low coagulant and low inflammatory bovine pericardium for surgical application.

1. Introduction

Xenogenic pericardial tissue, especially of bovine origin, is widely used to reconstruct defective structures in multiple surgical disciplines. Bovine pericardium also is the primary source used for biological aortic valve (AV) prostheses and patch materials in cardiac surgery [1–4]. Fixation with glutaraldehyde is the gold standard in the preparation of this tissue, as it stabilizes the tissue matrix by crosslinking the ECM-component collagen, at least in part inactivates xeno-epitopes, and has antiviral and antimicrobial properties. But this preparation strategy is also described to be responsible for the degeneration of AV-prostheses 10–15 years after implantation with the necessity for re-operation [5,6]. Reason for deterioration, often calcification of the tissue matrix, is seen in the incomplete crosslinking of glutaraldehyde (GA) at amine groups of collagen lysine residues and remaining free aldehyde groups [1,7,8]. The reduced longevity and toxicity concerns regarding AV bioprostheses and patches motivated to seek alternative fixation methods.

Multiple alternative crosslinking preparation strategies for bovine pericardium are published reaching from the application of crosslinking

Abbreviations: GA, glutaraldehyde; AV, aortic valve; ECM, extracellular matrix; LEEI, low-energy electron irradiation; UV, ultraviolet; α-Gal, galactosyl-α-1,3-galactose.

* Corresponding author at: Department of Cardiac Surgery, Carl Gustav Carus Faculty of Medicine, Technische Universität Dresden, Heart Centre Dresden, Fetscherstrasse 76, 01307 Dresden, Germany.
E-mail address: Claudia.Dittfeld@tu-dresden.de (C. Dittfeld).

[1] Contributed equally.

Provided by Sächsische Landesbibliothek, Staats- und Universitätsbibliothek Dresden

Final edited version was published in Biomaterials advances. 2023. 147. Elsevier. ISSN: 2772-9508..
https://doi.org/10.1016/j.bioadv.2023.213328

substances such as EGDE (ethylene glycol diglycidyl ether), EDAC (1-ethyl-3-(3-dimethylaminopropyl)-carbodiimide), genipin, curcumin or tannic acid [1] or using photosensitization or oxidation [9–11]. More recently ribose or innovative decellularization combined with EDAC but also furfuryl glycidyl ether in combination with Rose Bengal and involving photooxidation are supposed as new crosslinking methods [12–14]. Also strategies using riboflavin/UV after divers' pretreatment protocols were part of the numerous panel of published crosslinking procedures [15,16]. The so called PhotFix® patch, product of photo-oxidation, is in clinical use already [1,9]. Another alternatively prepared patch is the CardioCel® patch for which a glutaraldehyde-fixation with a very low concentration is performed in addition to a decellularization step [17,18]. Nevertheless, the clinical acceptance for alternatively treated patch materials is low and clinical data and results are indifferent [17–19]. A decellularized porcine heart valve prosthesis (Synergraft tissue engineered) failed for the application in children [20]. Long-lasting decellularization steps can lead to bacterial contamination, and examination of the endotoxin content is recommended. Endotoxin level references determine the limit at 0.5 EU/mL (extract) and 20 EU (device) [21].

For GA-free protocols, however, decellularization is essential because inflammatory and immunogenic xenogeneic epitopes or molecules, such as the carbohydrate moiety galactosyl-α-1,3-galactose (α-Gal), or Neu5Gc glycolyl form of neuraminic acid (Neu5Gc) as well as DNA have to be eliminated [22–24]. A DNA threshold of 50 ng doublestrand DNA (not longer than 200 bp) per mg ECM-dry weight has been defined, and the histological evaluation of the remaining nuclei is required [25]. Also the quantification of the remaining α-Gal epitope in the matrix is a further endpoint often examined [26]. Even protocols preparing porcine aortic valves without matrix crosslinking but solely intense decellularization protocols, including removal of N-linked glycans and DNA by enzymatic PNGase F and DNase I treatment, result in a low degree of inflammation in a sheep model [27]. Therefore an effective removal of DNA and partial deglycosylation can overcome rapid destruction of xenogeneic tissues, and protocols can be developed intensely investigating immune response [27–29]. Immune reactions against xenoantigens are driven by preformed IgM antibodies, activating the complement system, leading to an immediate response [30,31]. These rapid reactions make in vitro incubation assays with human whole blood a powerful tool for first-line evaluation of xenograft developments [32–34]. As these xenoantigens are expressed also by rodents typically used for in vivo biocompatibility evaluation, immune reactions would not appear in these animals, requesting tests in human blood. Comparable to the analysis of non-biological material, plasmatic and cellular parameters of hemostasis and inflammation can be examined after incubation in a semistatic system [35–37]. These parameters reflect the endpoints, also stated in the guidance of the International Organization for Standardization (ISO 10993-4) for the testing of medical materials with blood contact regarding hemocompatibility [33].

Combining decellularization with novel crosslinking and sterilization strategies, the SULEEI (stabilize and sterilize [S] acellular pericardial scaffolds combining photo-initiated ultraviolet crosslinking [U] with low-energy electron irradiation [LEEI])-procedure was introduced to prepare porcine pericardium in a GA-free manner [38]. After decellularization of the pericardium with Triton X-100, DNase and RNase, crosslinking of collagen was realized by UV-irradiation in riboflavin solution, similar to the protocol established for the crosslinking of the collagen-rich cornea in ophthalmology and also suggested for cosmetic applications using blue light [39–43]. Riboflavin/UV treatment is further suggested to optimize the preparation of decellularized human arterial small-diameter vascular grafts [44]. Riboflavin is the inducer of the standard photochemical reaction that in combination with UVA results in reactive oxygen species and these in turn result in covalent crosslinking of (pericardium) collagen fibers, elastin and proteoglycans [16,43,45]. Beside this oxygen mediated crosslinking, riboflavin can be transformed into a triplet state due to UVA light absorption creating covalent bonds between collagen fibrils as well [42]. In addition, glycosylative crosslinking between proteoglycans and collagen via advanced glycation end product-mediated mechanisms are described [42]. In the presented work, this technology has been combined with low-energy electron beam irradiation to the SULEEI-procedure for additional crosslinking along with sterilization of the tissue matrix [38]. Bovine pericardium was treated with the same protocol as developed for porcine pericardium, and comparable results for biomechanics and histological features were observed [15]. However, the higher thickness of the tissue but also an increased susceptibility for in-process bacterial contamination caused practical challenges concerning the decellularization and penetration of the low energetic electrons and demanded adaptation and improvement of the protocol [15,38].

Two different protocols were compared: (A) decellularization with DNase and RNase only before Triton X treatment and 10× concentration of riboflavin and dextran (related to previous study) [38]. (B) decellularization with additional trypsin but original riboflavin and dextran concentration. Pericardia treated with the two protocols were tested in human whole blood incubation for inflammatory and coagulant responses. According to resulting findings an optimized treatment protocol SULEEI-C was developed and evaluated along with the intermediate preparation steps. Detailed hemocompatibility test setup facilitates essential improvement of GA-free SULEEI-preparation strategy featuring excellent biomechanical properties combined with optimal immunological prerequisites of bovine pericardium for long term surgical application.

2. Materials and methods

2.1. Preparation of SULEEI-pericardia

Bovine pericardial sacs from two to nine year-old cattle were obtained from a local slaughterhouse (Vorwerk Podemus ökologischer Landbau, Dresden, Germany) and transported immediately to the laboratory. The surrounding fatty and connective tissues were removed, the pericardium was washed several times with phosphate-buffered saline (PBS), divided into different segments and stored for 60 h in 5 mM tris (hydroxymethyl)aminomethane (Tris; pH 8; 4 °C) containing 2 % phenoxyethanol to prevent bacterial growth and keep endotoxin levels in the permitted range. Subsequently, segments were assigned to various pretreatment strategies according to the SULEEI or GA-fixation process. The SULEEI-protocol is a three-step process (Fig. 1; adapted from Walker et al. 2020 [15]) and is summarized in Table 1 demonstrating the adaptations in protocols B and C. In brief for protocol B, pericardia were treated 5-mM Tris buffer containing 1 % Triton-X 100 (SERVA Electrophoresis GmbH, Heidelberg, Germany) for 8 h at 4 °C. Subsequently, tissues were washed twice with Hank's BSS (Carl Roth GmbH & Co. KG, Karlsruhe, Germany) with Ca^{2+} and Mg^{2+} for 15 min at 4 °C. Enzymatic digestion was performed with DNAse (0.1 mg/ml), RNAse (0.02 mg/ml; both from SERVA Electrophoresis GmbH), and trypsin (0.004 mg/ml) (Biochrom, Berlin, Germany) diluted in Hank's BSS at 37 °C for 15 h. The pericardia were then transferred to 5 mM Tris buffer (pH 8) supplemented with 1 % Triton-X 100 and incubated for 7 h at 4 °C. Finally, pericardial tissues were washed four times with PBS at 4 °C and incubated in PBS until analysis. The protocol was adapted according to Roosens et al. [46]. Subsequently, pericardia were incubated in 260 μM riboflavin-5′-phosphate monosodium salt/2 % dextran in PBS for 1 h at 4 °C. Then, fibrous and serous sites were treated with UV radiation (365 nm, 0.3 mW/cm^2; UVA lamp UVL-28 EL Series, Analytik Jena, Jena) for 3 h each. After washing in PBS at 4 °C for four times, a semi-dry status was achieved by pressing between filter paper sheets for 10 min. For irradiation, pericardial samples were wrapped in polyethylene foil. To ensure a sustainable level of sterility, samples were irradiated with low-energy electron irradiation at atmospheric pressure with an accelerating voltage of 200 kV, a current of 3 mA, and a dose of 36 kGy (KeVac System, Linac Technologies, Orsay, France [200 kV, 5 mA]) from both

Provided by Sächsische Landesbibliothek, Staats- und Universitätsbibliothek Dresden

Final edited version was published in Biomaterials advances. 2023. 147. Elsevier. ISSN: 2772-9508..
https://doi.org/10.1016/j.bioadv.2023.213328

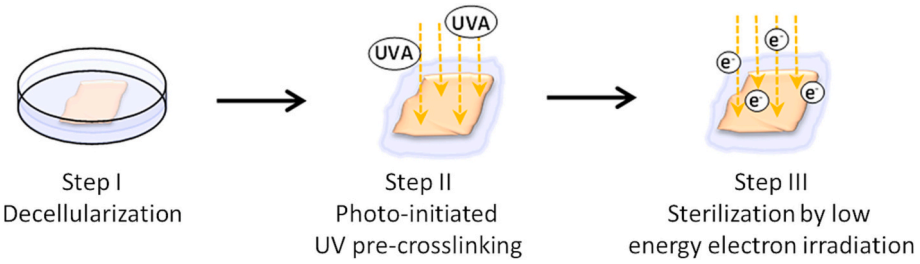

Fig. 1. Schematic diagram of the SULEEI procedure [38]. After decellularization of pericardial tissue (step I), pericardia were soaked in riboflavin and UV irradiated (step II) and finally treated with low-energy electron irradiation (step III). UV, ultraviolet; LEEI, low-energy electron irradiation.

Table 1
SULEEI-preparation protocol and adaptations for protocols A, B and C.

	SULEEI A	SULEEI B	SULEEI C
Decellularization	–	1 % triton X-100 in 5 mM Tris (pH 8), 4 °C, 8 h	
	2 × Hank's BSS with Ca^{2+} and Mg^{2+}, 15 min, 4 °C		
	0.1 mg/mL DNAse, 0.02 mg/ml RNAse in HBSS, 37 °C, 4 h	0.1 mg/mL DNAse, 0.02 mg/ml RNAse, 0.004 mg/mL trypsin in HBSS, 37 °C, 15 h	
	1 % triton X-100, 5 mM Tris (pH 8), 4 °C, up to 1 h	1 % triton X-100 in 5 mM Tris (pH 8), 4 °C, 7 h	
	4 × PBS, 30 min		
Stabilization	2.67 mM riboflavin-5′-phosphate monosodium salt, 20 % dextran in PBS, 4 °C, 1 h	260 µM riboflavin-5′-phosphate monosodium salt, 2 % dextran in PBS, 4 °C, 1 h	260 µM riboflavin-5′-phosphate monosodium salt in PBS, RT, 1 h,
	UVA-irradiation (365 nm) with 1.5 mW/cm², 1 h, fibrous and serous side	UVA-irradiation (365 nm) with 0.3 mW/cm², 3 h, fibrous and serous side	UVA-irradiation (365 nm) with 3 mW/cm², 1 h, fibrous and serous side
	4 × PBS, 30 min		
Sterilization	Dehydration process to semi-dry status by incubation in filter paper, 10 min		
	Transfer into HDPE (high density polyethylene) foil		
	Low-energy electron irradiation, atmospheric pressure, accelerating voltage of 200 kV, current of 3 mA, dose of 36 kGy, fibrous and serous side		

sides. The absorbed dose was measured in parallel with a radiochromic dosimeter film (Risø B3 dosimeter, Risø High Dose Reference Laboratory, Roskilde, Denmark).

GA-fixation was performed for 3 h at room temperature (RT) with bovine pericardium from the same individual using 0.625 % GA diluted in 20.4 mM HEPES-buffer supplemented with 13 mM $MgCl_2 \times 6\ H_2O$ and 80.6 mM NaCl (pH 7.4). Native control pericardia were incubated in PBS buffer at 4 °C until the experimental setup was started.

2.2. Quantification of DNA

In order to quantify dsDNA in the pericardial tissue samples, tissue extraction with Proteinase K was carried out, followed by purification using the spin column-based DNeasy Blood & Tissue Kit (Qiagen). The dsDNA was detected in the purified extract with the dsDNA High Sensitivity Fluorescent Assay Kit (DeNovix). The fluorescence was measured by MTP-Reader (Infinite® 200, Tecan) at 464 nm excitation and 550 nm emission wavelength. Accordingly, ssDNA and dsDNA was detected by Qubit ssDNA Assay Kit (Thermo Fisher Scientific) and fluorescence was measured using the Qubit 2.0 fluorometer (Invitrogen). The ss or dsDNA content was expressed as ng ss or dsDNA/mg dry tissue weight. At least three individual pericardium preparations of SULEEI-A, SULEEI-B and SULEEI-C were investigated in comparison to native tissue.

To estimate the fragment length, the extracted dsDNA from the decellularized tissue samples was separated by gel electrophoresis in a 3 % agarose gel in TBE buffer. As references, 5 µl GeneRuler Ultra Low Range DNA Ladder (300–10 bp, Thermo Scientific) in 1 µl 6× TriTrack DNA Loading Dye (Thermo Scientific) and 5 µl PCR Ladder (3000 bp–100 bp, VWR) and 5 µl 5× Loading Buffer Blue (VWR) mixed as described above were used. The dsDNA samples were prepared in the same way as the high range PCR Ladder. After loading the samples, the gel was run at 130 V for 90 min and dark-incubated for 30 min in a staining bath containing 150 µl GelRed Nucleic Acid Stain (10,000× in water, VWR) and 500 ml dH_2O. The stained dsDNA was visualized with a gel documentation system (biostep), including a DH-50 dark hood, a 312 nm UV transilluminator and the Argus X1 software.

2.3. Histological analysis and quantification

Histological evaluation was carried out in order to analyze morphological differences between all pericardia and the different preparation steps, the different SULEEI-protocols vs. native and GA-fixed tissue. For this, pericardia were fixed in 4 % buffered formalin in PBS and embedded in paraffin. Slices of 3 µm thickness were stained by standard hematoxylin/eosin (HE) and picrosiriusred staining protocol to evaluate the effect of decellularization and collagen fiber density. Samples were digitalized using the slide scanner (Axio Scan.Z1, Carl Zeiss Microscopy GmbH, Jena, Germany). Collagen content was quantified on picrosiriusred stained sections with Fiji-software using the color deconvolution plugin and user threshold values. The picrosiriusred positive area was quantified in relation to total section area ($n \geq 5$ individual bovine pericardial tissues for native, SULEEI-pericardium, and glutaraldehyde fixed control; average from at least two sections per sample [area 5–15 mm^2]). For decellularized and decell/riboflavin/UV-treated tissues, at least four sections of two individual pericardia were examined. Remaining nuclei fragments and fragment area were determined after HE staining using Fiji software (color deconvolution plugin, user threshold values). Nuclei count was related to section area. Immunohistochemical detection of α-Gal (samples without hemocompatibility testing), CD15 (granulocyte marker), CD61 (platelet marker) and complement fragment C3b was performed according to

Table 2
Antibodies and staining conditions for immunohistochemistry.

Antibody	Company	Dilution	Buffer system	Isotype controls
α-Gal	ENZO (ALX8010001)	1:150 (conc. unknown)	Tris-EDTA, pH 9.0	IgM mouse (Santa Cruz, #sc3881)
CD15	DAKO (M3631)	1 µg/ml	Citrate buffer, pH 6.0	
CD61	Abcam (ab179473)	1 µg/ml	Citrate buffer, pH 6.0	IgG rabbit (Cell Signaling #3900)
C3/C3b/C3c	Proteintech (21337-1-AP)	0.15 µg/ml	Tris-EDTA, pH 9.0	

Provided by Sächsische Landesbibliothek, Staats- und Universitätsbibliothek Dresden

Final edited version was published in Biomaterials advances. 2023. 147. Elsevier. ISSN: 2772-9508..
https://doi.org/10.1016/j.bioadv.2023.213328

parameters shown in Table 2 and according to standard protocols using heat-induced epitope retrieval.

Infiltrated granulocytes in native, decellularized and SULEEI-pericardium were counted, excluding the top cover layer of pericardial samples after hemocompatibility testing. The number was rated to the tissue area. In addition, the distance of the infiltrated granulocytes from the blood incubated surface was measured using ZEN-Blue software version 3.3 (ZEISS, Germany).

2.4. Hemocompatibility testing

The whole blood incubation was performed as described previously [35]. Briefly: pericardial samples were used as top and bottom in in-house developed incubation chambers, where 2 ml blood are exposed to 6.3 cm^2 test material. Where discernable, the serous side of the pericardium was exposed to the blood, as pre-tests indicated better reproducible results due to the clearly defined surface. Identification of the sides was impeded for the decellularized samples without fixation. Glass and Teflon AF™ served as activating and inert reference materials.

Blood was obtained freshly by venipuncture from two healthy voluntary donors with blood group O, because this blood group is reported to show highest reactivity against the α-Gal epitope [47]. The donors did not take any medication during the recent ten days. The blood was immediately anticoagulated with 1.5 U/ml heparin (Ratiopharm, Ulm, Germany). The two donations were pooled after verifying that the blood cell count was within the reference values (Counter AcT diff, Beckman Coulter, Krefeld, Germany) and that C-reactive protein was below 10 mg/l (PoC test, möLab, Langenfeld, Germany). The pooled blood was filled in the incubation chambers without air interface, and the chambers were incubated at constant overhead rotation for 2 h at 37 °C.

After incubation, the chambers were opened, and blood was analyzed for blood cell count. Blood was stained for flow cytometric analysis (LSR Fortessa, BD Biosciences, Heidelberg, Germany) of CD11b expression (CD11b-PacificBlue, BioLegend, San Diego, CA, USA) on granulocytes, identified by the characteristic forward- and side scatter pattern and CD15 (CD15-PE, BioLegend) positivity. Further, blood was stabilized with recommended anticoagulants for ELISA analysis of platelet factor 4 (PF4, Zymutest PF4, CoaChrom, Vienna, Austria), prothrombin fragment F1 + 2 (Enzygnost F1 + 2 micro, Siemens Healthineers, Eschborn, Germany), and complement fragment C5a (DRG Instruments, Marburg, Germany), spun down, and the supernatant was stored at − 80 °C till further analysis. The pericardial samples were rinsed blood-free with PBS and then either fixed with 2 % glutaraldehyde in PBS, dehydrated in increasing ethanol concentrations critical-point dried and inspected in SEM or prepared for histological analysis as described above.

Two independent incubations with different blood donors were performed for each set of samples. In each experiment, a triplicate set of samples was incubated (total $n = 6$).

2.5. Enzymatic digestion

The stability against enzymatic degradation was analyzed in glutaraldehyde-fixed and SULEEI-treated bovine pericardia by digestion with 0.4 PTZ U/mL Collagenase NB8 Broad Range (SERVA Electrophoresis GmbH) in 50 mM Tris buffer for 8 h. Tissue weight was measured before and after digestion related to the initial weight of each sample.

2.6. Uniaxial tensile test

Biological pericardium replicates ($n \geq 3$) using three different tissue areas per sample of native, GA-fixed and SULEEI (A-C) were cut into 10 × 15 mm rectangles. Tissue thickness was measured with the thickness gauge FD50 (Kaefer Messuhrenfabrik GmbH & Co. KG, Villingen-Schwenningen, Germany). Ends of the tissue samples were fixed into the wedges of the Minimat Miniature Materials Tester (Polymer Lab., Dresden, Germany). A pre-load of 0.02 N and resulting clamping lengths of 7.0–8.5 mm were adjusted. Tensile testing was performed with a deformation rate of 4 mm/min until a tensile force of 10 N or an elongation of 10 mm was reached. After stress-strain curves were plotted, the Young's modulus (E) was evaluated as the slope of the linear function of the respective stress-strain curve.

2.7. Determination of sGAG, hydroxyprolin and elastin

The amount of sulfated glycosaminoglycans (sGAG) in pericardial tissue was determined in the supernatant after performed papain extraction. Firstly, the biological tissues were digested at 65 °C for 4 h with a papain extraction reagent containing sodium dihydrogen phosphate dihydrate, sodium acetate, EDTA, cysteine hydrochloride and papain (449 U/ml). After centrifugation for 10 min, the supernatant was mixed with dimethylmethylene blue (DMMB) dye reagent and incubated at room temperature in darkness for 30 min. The absorbance at 595 nm was measured, indicating the sGAG amount by MTP-Reader (Infinite® 200, Tecan). Calibration was performed with chondroitin sulfate. The sGAG content of the samples was expressed as µg sGAGs/mg dry tissue weight.

Hydroxyproline assay was performed to quantify collagen content in native, GA-fixed and SULEEI-treated bovine pericardium according to Creemers et al. [48]. Therefore, 10 mg of dried tissue were incubated in 10 N NaOH for 1 h at 120 °C followed by neutralization in 10 N HCl. After centrifugation (10,000 ×*g*, 5 min), the supernatant was diluted 1:80 and assayed in duplicate. After reaction with chloramine T and DMAB the extinction was measured at 570 nm with a reference wavelength of 655 nm.

Fastin™ Elastin assay (Biocolor Ltd., Northern Ireland, United Kingdom) was performed to quantify elastin content in native and SULEEI-treated bovine pericardium. Prior to assay elastin was extracted from tissue samples by placing 10 mg of dried tissue in 0.25 M oxalic acid. After incubation at 100 °C for 1 h, samples were centrifuged at 10,000 rpm for 10 min. The supernatant was pipetted off and retained for analysis. Two more heat extractions were performed with the residual tissue. For analysis, the supernatants from the first and second heat extraction were pooled, whereas the third extract was measured separately to establish that elastin extraction was quantitative. For elastin precipitation sample volumes of 50 and 100 µl were used and the assay protocol was performed as per manuals instruction.

2.8. Calcification potential in vitro

Native, GA-fixed and SULEEI-C pericardia were incubated in simulated body fluid mSBF [49,50] (5 ml 2× mSBF/cm^2) for up to 27 days. Calcium content was determined after 48 h incubation of pericardia in 2 M HCl solution in RT using the o-cresolphthalein-complex formation method and photometric detection at 575 nm. Calcium content was related to dry weight.

2.9. Statistical assessment

Unless indicated otherwise, whole blood incubations was performed with a triplicate set of tissue samples obtained from the same pericardium and pooled blood of two donors. The experiments were repeated once with different pericard and blood donors, resulting in $n = 6$ analyses. Data are presented as mean ± standard deviation. Tests for statistical differences were performed with analysis of variance (ANOVA) or ANOVA on ranks, as appropriate, and subsequent post-hoc analysis according to Student-Newman-Keuls or Tukey, respectively, using the software SigmaPlot (Inpixion, Palo Alto, CA, USA). Quantification of histological, biochemical and calcification parameters was statistically tested with analysis of variance (ANOVA) applying post-hoc analysis

Provided by Sächsische Landesbibliothek, Staats- und Universitätsbibliothek Dresden

Final edited version was published in Biomaterials advances. 2023. 147. Elsevier. ISSN: 2772-9508..
https://doi.org/10.1016/j.bioadv.2023.213328

according to Tukey or Dunnett's multiple comparisons test. At least three individual pericardium preparations were investigated for native and GA-fixed pericardia and SULEEI samples A, B or C, in triplicates. Two individual pericardia of intermediate protocol step conditions (decell or decell/riboflavin/UV) were included evaluating at least four histological sections in this cases. Number of samples analyzed are indicated in the results section.

3. Results

3.1. Histological evaluation of SULEEI-pericardium A and B

Two SULEEI protocols, A and B, were applied for the treatment of bovine pericardium. Protocol A is characterized by an elevated riboflavin/dextran concentration in the UV step, and B is characterized by the generally more extended and more intense, trypsin-containing decellularization step.

To characterize the SULEEI-tissue properties, collagen fiber density, α-Gal positivity and nuclei fragments were quantified. Collagen fiber density was with 86.6 ± 4.2 % significantly higher in SULEEI-B pericardium compared to native control (76.0 ± 9.4 %; Fig. 2a; $n \geq 5$). A tendency for a higher picrosiriusred positive fiber density of SULEEI-A pericardium (85.7 ± 5.0 %; $p < 0.1$) compared to native tissue was monitored. GA-treated tissue did not differ from native tissue (Figs. 2 and 3a).

The xenoepitope α-Gal was visualized by immunohistochemistry (IHC), and quantification of IHC-positive area revealed with a value of 0.044 ± 0.008 % a significant reduction in SULEEI-B tissue in comparison to native (0.47 ± 0.35 %) or GA-fixed tissue (0.49 ± 0.24 %; Figs. 2 and 3b; $n \geq 4$).

The double-strand DNA-content, investigated after digestion of the tissue matrix, was below 15 ng/mg dry weight for all SULEEI-preparations. However, the detection of double and additional single-strand DNA resulted in 39.6 ± 43.2 ng/mg dry weight in SULEEI-A and 29.8 ± 15.8 ng/mg dry weight in SULEEI-B, which is higher but still below the 50 ng/mg dry weight threshold [25] (not shown). Nuclei fragments were visible after HE-staining and quantified (Figs. 2 and 3c). With 109.7 ± 102.4 (A) and 0.3 ± 0.3 (B) nuclei or fragments per mm^2, respectively, both SULEEI-pericardia exhibit a significant reduction in comparison to the native or GA-fixed tissues (445.0 ± 199.2 nuclei/mm^2 and 417 ± 163.2 nuclei/mm^2; Fig. 2c; $n \geq 5$). Direct comparison between the two SULEEI-protocols revealed significant differences with higher values in SULEEI-A in the total count per area (not shown) but with 5.9 ± 1.2 and 4.4 ± 1.2 μm^2 comparable fragment areas ($n = 3$; not shown; in two SULEEI-B samples no nuclei detectable). Nuclei area in native and GA-fixed pericardial tissues was with 11.5 ± 1.0 and 10.0 ± 1.4 μm^2, respectively, significantly higher (not shown). DNA gel electrophoreses support the results of this quantification. In SULEEI-A sample DNA fragments sizes between 300 and 50 bp were detectable (Fig. 2d). From these results, it can be summarized that the more gentle decellularization step without trypsin in protocol A was less efficient. The effect of both protocols on the activation of inflammatory and coagulant processes in whole blood should be evaluated in the next step.

3.2. Analysis of hemocompatibility of SULEEI-A and SULEEI-B pericardium

Hemolysis was not observed after any whole blood incubation, indicating that no residual detergents, toxic riboflavin concentrations or free radicals were released. The native pericardium induced very high activation of the plasmatic coagulation, measured as thrombin activation (prothrombin fragment F1 + 2 release, Fig. 4a), comparable to the positive control glass. GA treatment pressed this activation to the level of the inert control Teflon AF™ ($p < 0.05$). The trypsin-free, ECM preserving protocol SULEEI-A induced even higher coagulation activation than the native pericardium. The SULEEI-B protocol substantially pressed the

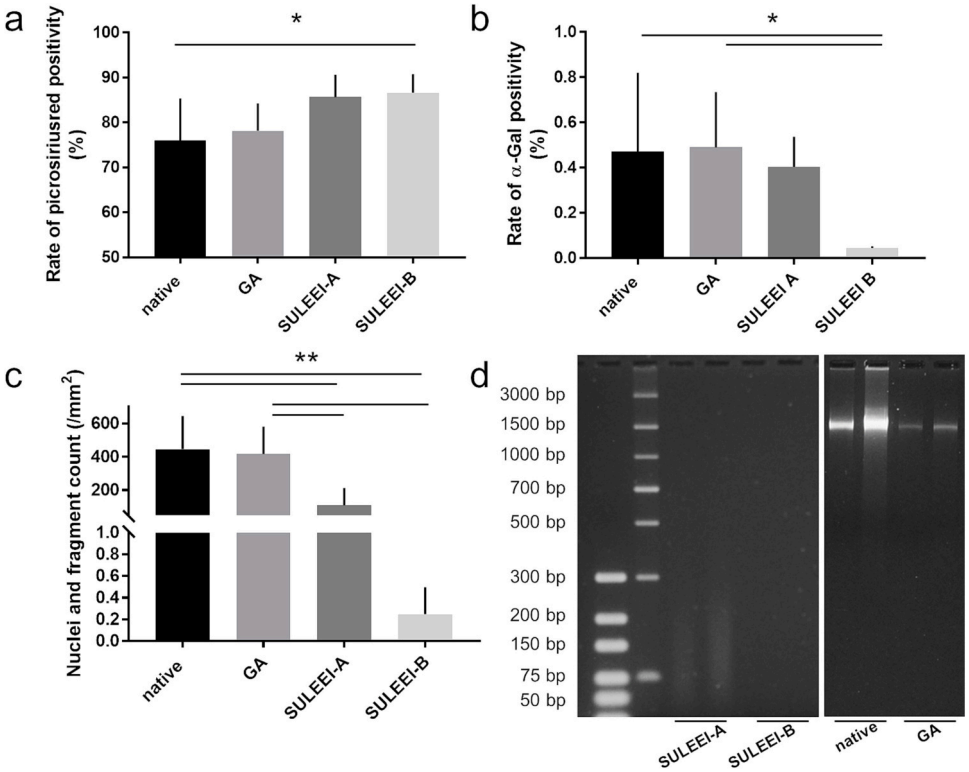

Fig. 2. Quantification of collagen fiber density (a), α-Gal positive areas (b) and remaining nuclei or nuclei fragments (c) of bovine pericardia treated with the trypsin-free SULEEI-A vs. trypsin-containing SULEEI-B protocol in comparison to native and GA-fixed counterparts. DNA fragment size of 300 to 50 bp was detected in SULEEI-A samples via gel electrophoresis in two independent pericardium preparations (d) a–c) One-way ANOVA, Tukey-Test; *$p < 0.05$; **$p < 0.01$.

Provided by Sächsische Landesbibliothek, Staats- und Universitätsbibliothek Dresden

Final edited version was published in Biomaterials advances. 2023. 147. Elsevier. ISSN: 2772-9508..
https://doi.org/10.1016/j.bioadv.2023.213328

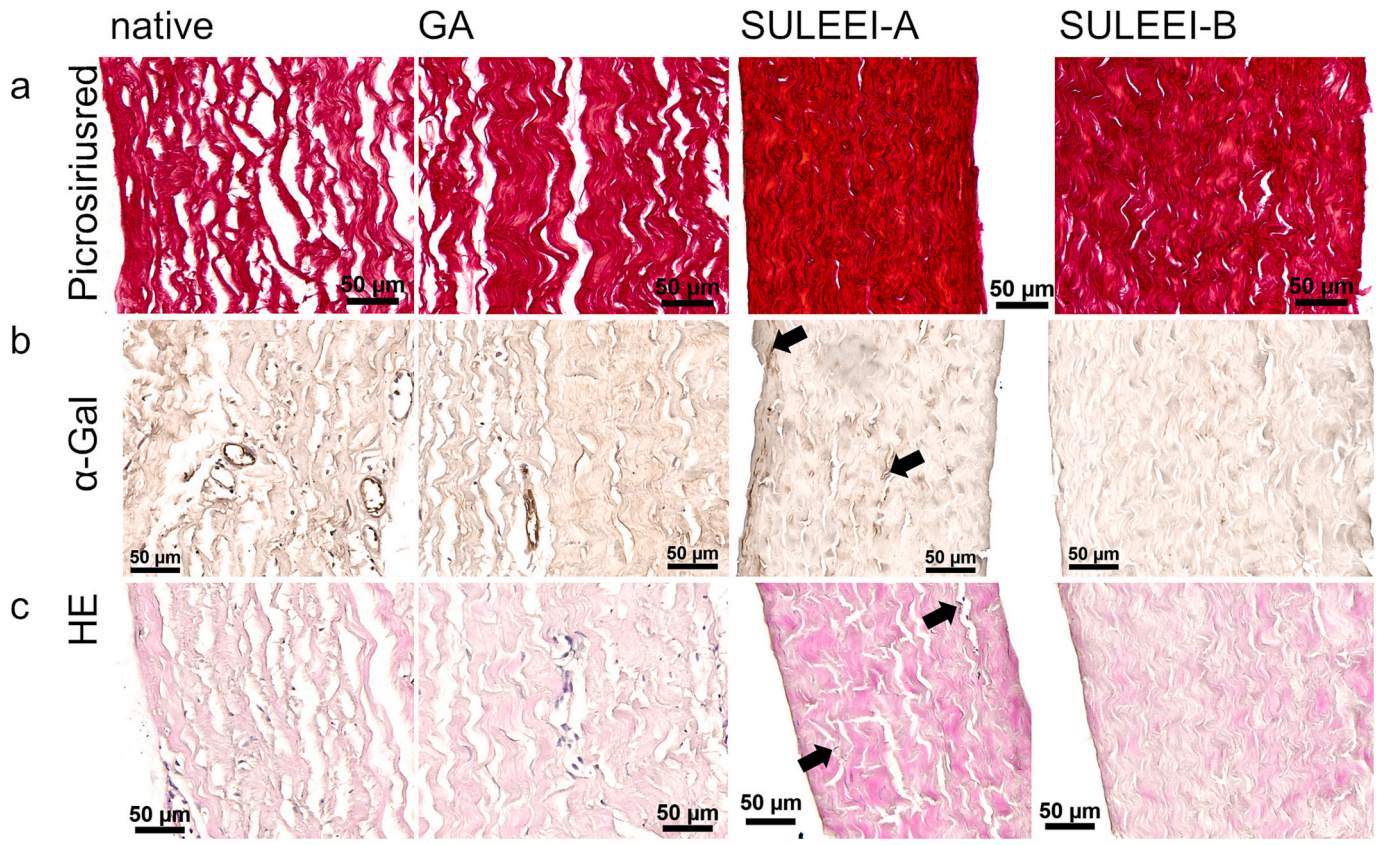

Fig. 3. Histological evaluation of SULEEI-A and SULEEI-B pericardia in comparison to native and GA-fixed tissue. Enhanced collagen fiber density was visualized in picrosiriusred staining of SULEEI treated pericardium (a). Remaining cellular fragments (arrows) were detected in α-Gal via immunohistochemistry (b) and in HE-staining (c) in SULEEI-A tissue.

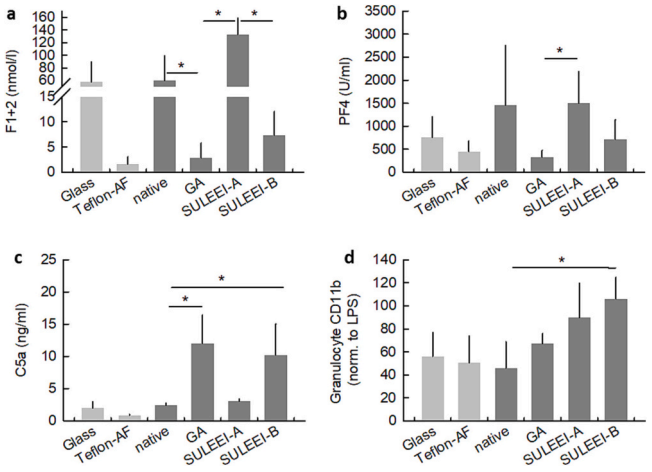

Fig. 4. Activation of hemostatic and inflammatory processes in whole blood after incubation two or with native, glutaraldehyde fixed pericardium (GA), and pericardium prepared according to SULEEI protocols (A) and (B). Glass and Teflon AF serve as reference materials. (a) Prothrombin fragment F1 + 2 as marker of plasmatic coagulation. (b) Platelet factor 4 (PF4) as marker of platelet activation. (c) Complement fragment C5a as marker of complement activation, and (d) CD11b expression on granulocytes as marker of cellular inflammation. Data presented as mean ± SD of n 6 incubations. Asterisks indicate differences with $p < 0.05$, ANOVA on variance, with Tukey post hoc analysis.

coagulation from the native pericardium to values only slightly exceeding the GA control. F1 + 2 concentration of SULEEI-B was significantly lower than SULEEI-A ($p < 0.05$).

Thrombin is the strongest activator of blood platelets, therefore concentrations of the platelet activation marker PF4 (Fig. 4b) mainly followed the trends of the F1 + 2 concentration. Native and SULEEI-A treated samples induced high PF4 release, both exceeding the glass control. Platelet activation was suppressed after the GA treatment and to a lower extent after SULEEI-B treatment. These data are supported by the reduced platelet count in the blood phase after incubation due to adhesion to the pericardial surface or to other blood cells (Suppl. Fig. 2a).

Complement cascade activation as an inflammatory response was measured as the release of the complement fragment C5a (terminal pathway of the complement cascade, Fig. 4c). While native and SULEEI-A treated pericardium induced only low levels of complement activation, GA treatment and SULEEI-B treatment with the more gentle riboflavin/UV treatment step induced clearly elevated complement activation.

C5a is the strongest activator of granulocytes and monocytes; however, leukocyte activation in this study, measured as CD11b expression (Fig. 4d), showed low correlation with the C5a concentration. The CD11b expression on granulocytes was higher for the SULEEI fixed samples. Non-identified additional activation processes may play a role. SULEEI-A caused higher loss of granulocytes from the blood than SULEEI-B (Suppl. Fig. 1). Probably, this loss of cells due to adhesion to the surface mainly affected highly activated cells, and therefore, the CD11b level of the remaining cells in the blood was lower.

To support these results, pericardial tissue was investigated by immunohistology for CD15 and CD61 positivity of the surface covering after hemocompatibility testing and in comparison to pre-

Provided by Sächsische Landesbibliothek, Staats- und Universitätsbibliothek Dresden

Final edited version was published in Biomaterials advances. 2023. 147. Elsevier. ISSN: 2772-9508..
https://doi.org/10.1016/j.bioadv.2023.213328

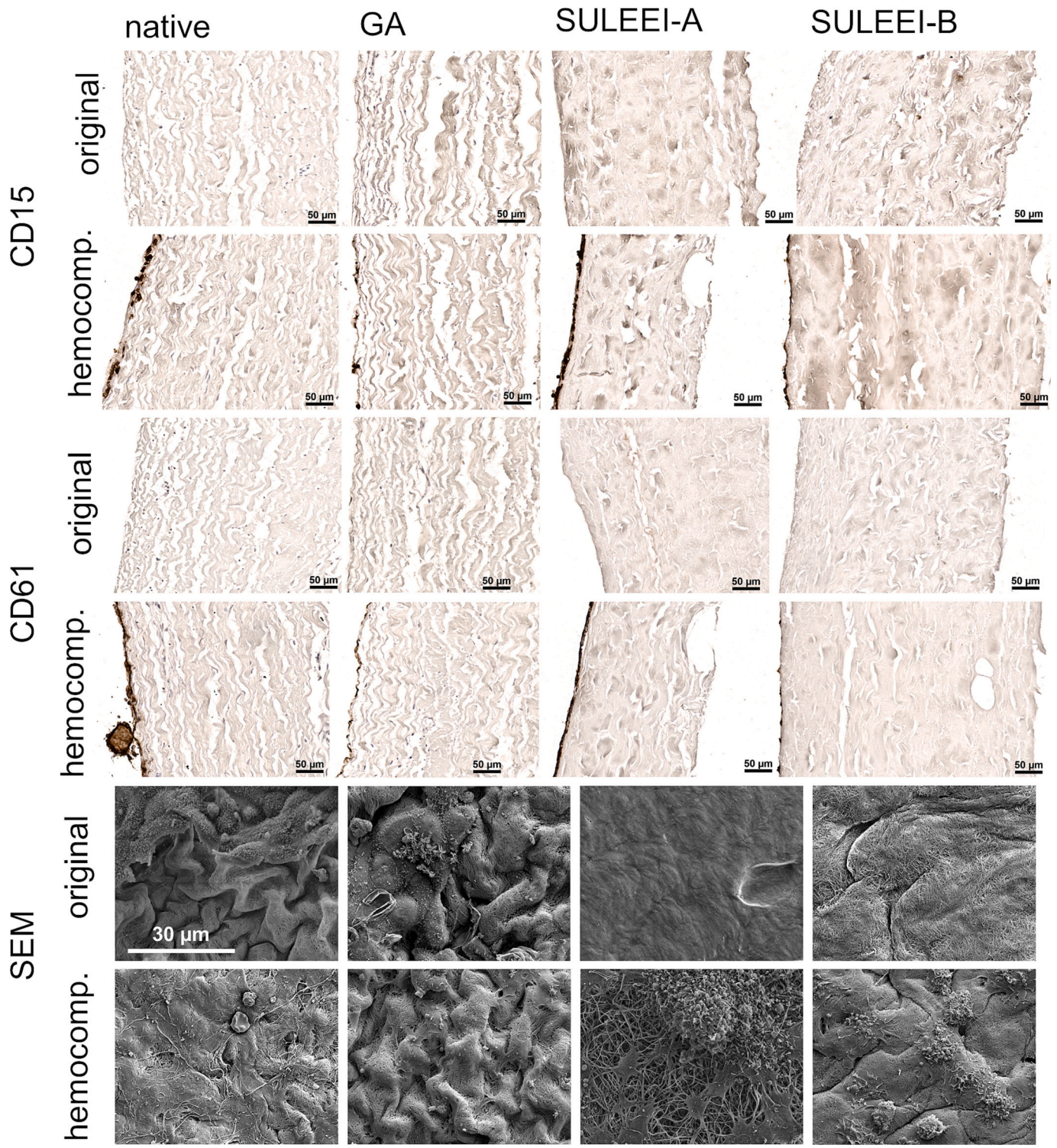

Fig. 5. Investigation of SULEEI-A and B treated pericardia after hemocompatibility incubation in comparison to native and GA-fixed and non-incubated (original) counterparts by histology and SEM. Dense fibrin covering on the serous, blood-contacting side of native and SULEEI-A treated pericardium after blood incubation was detected, containing CD15 positive granulocytes and CD61 positive platelets.

hemocompatibility samples (Fig. 5). CD15 is a marker for granulocytes, and CD61 is a marker for thrombocytes. As expected, both antigens were detected on native pericardium samples after blood incubation, and within the dense protein- and cell layer covering the SULEEI-A treated tissue (Fig. 5). GA-fixed and SULEEI-B prepared counterparts also exhibited CD15 and CD61 positivity of the covering layer, yet less compact and containing some free areas. SEM analysis of the samples, on the one hand, allows the assessment of the ECM surface structure in the pre-hemocompatibility samples and, on the other hand, the evaluation of the deposited cell- and protein layer after blood incubation (Fig. 5). Collagen surface, partly with residual mesothelial cell layer (native sample), was visible in the pictures of original tissues before blood exposure. Surfaces of SULEEI samples appeared smoothened and even due to the filter drying step before the low-energy-electron-irradiation.

Provided by Sächsische Landesbibliothek, Staats- und Universitätsbibliothek Dresden

Final edited version was published in Biomaterials advances. 2023. 147. Elsevier. ISSN: 2772-9508..
https://doi.org/10.1016/j.bioadv.2023.213328

GA-fixed material exhibited preparation-based debris. After hemocompatibility testing, a dense 3D fibrin mesh was detected on SULEEI-A treated pericardium. In addition, a platelet-containing thrombus was shown (Fig. 5). Adherent platelets were visible with high density on native pericardium and more sporadically on the surface of GA-fixed and SULEEI-B-treated pericardia.

3.3. Optimized SULEEI-C protocol and analysis of intermediate products

Due to the complete decellularization, the nearly entire absence of nuclear fragments and α-Gal epitope, the trypsin-containing decellularization protocol according to SULEEI-B was chosen for further optimization. Dextran in the riboflavin/UV irradiation step appeared to enhance blood activation. Therefore dextran was omitted, and the riboflavin concentration was reduced in the riboflavin/UV stabilization step in protocol SULEEI-C.

Histological evaluation of the resulting SULEEI-C pericardium revealed a non-significant trend of enhanced collagen fiber density (91.2 ± 3.5 %) compared to native (82.8 ± 9.0 %; $n = 5$) or GA-fixed (84.0 ± 6.1 %) pericardium (Fig. 6 and Suppl. Fig. 2a). After decellularization, with 73.0 ± 16.0 %, the fiber density was reduced compared to the native matrix coherent with the visual impression in histological sections (Fig. 6b and Suppl. Fig. 2). After crosslinking by riboflavin/UV and the complete SULEEI-C protocol, the fiber density was 87.6 ± 2.2 % and 90.79 ± 4.5 %, respectively, significantly higher than in native or GA-fixed tissue (5 sections of $n = 2$). Decellularization of SULEEI-C was as efficient as in SULEEI-B protocol. Only 0.1 ± 0.1 nuclei or fragments per mm^2 were detected in pericardia after SULEEI-C treatment, significantly lower counts than in native or GA-fixed tissue and in the range of SULEEI-B pericardium (Fig. 6c, $n = 5$). Extensive washing processes accompanying the protocol after riboflavin/UV crosslinking, therefore, significantly reduced nuclei fragment count in SULEEI-C pericardia (5 sections of n = 2; Fig. 6d). The content of α-Gal positivity in IHC-stained tissues (Suppl. Fig. 2b) for SULEEI-C was comparable to SULEEI-B, with values of 0.04 ± 0.05 % (data not shown, n = 5).

Pericardium, prepared according to the optimized SULEEI-C protocol, was also tested for the response in whole blood. For further exploration of the activation mechanisms, also samples of the intermediate steps were exposed to blood (Fig. 7).

The trypsin-containing decellularization-step substantially reduced the hemostatic potential of the pericardium, as seen at the thrombin activation (F1 + 2), but the level of GA fixed sample was not achieved (Fig. 7a). The riboflavin/UV crosslinking step had no influence on the coagulation, but the final electron beam irradiation (sample SULEEI-C) tended to decrease the activating potential further, to or below the level of the GA fixation. Values of platelet activation (PF4) mainly confirmed the coagulation activation seen in the F1 + 2 levels (Fig. 7b). The platelet activation was pressed almost to the levels of the GA benchmark in the SULEEI-C treated sample.

Regarding the inflammatory response, decellularization induced high activation of the complement cascade, seen at the elevated C5a concentration (Fig. 7c). Riboflavin/UV crosslinking tended to reduce the complement activation, and the electron beam treatment reduced it further, close to the level of the initial and the controls. Granulocyte activation at the different SULEEI-steps, measured as CD11b expression (Fig. 7d), showed comparable trends as the complement activation with highest activation by the decellularized sample, and suppressed activation after riboflavin/UV crosslinking and further after the electron beam irradiation.

After human whole blood incubation, samples were investigated by

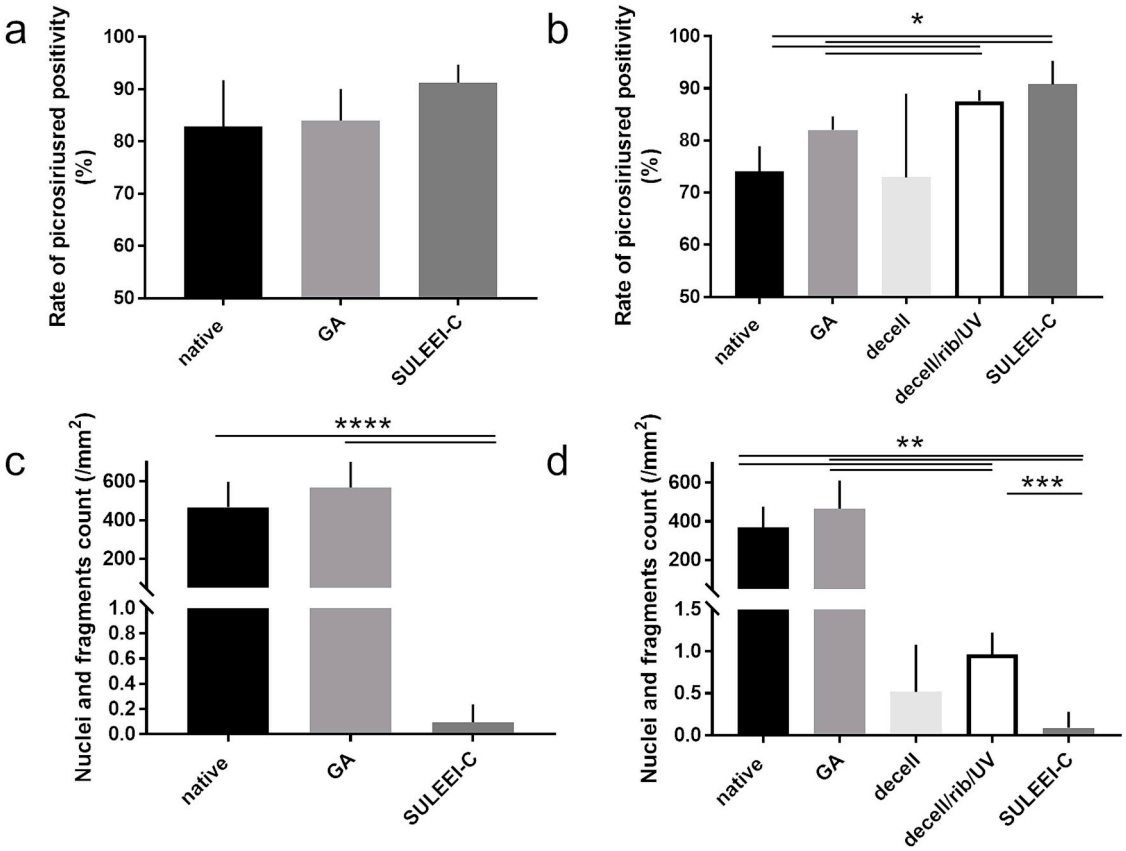

Fig. 6. Verification of collagen fiber density and absence of nuclei or nuclear fragments in the adapted SULEEI-C protocol (a; n 5), including intermediate pericardial material after decellularization and after additional UV-irradiation in riboflavin (b; n 2). In SULEEI-C tissue, the fiber density was not significantly enhanced. Nuclear fragments in SULEEI-C pericardium were significantly reduced below to SULEEI-B level (c; n 5, d n 2). One-way ANOVA, Tukey-Test; *$p <$ 0.05; **p < 0.01; ***$p <$ 0.005; ****$p <$ 0.0001.

Provided by Sächsische Landesbibliothek, Staats- und Universitätsbibliothek Dresden

Final edited version was published in Biomaterials advances. 2023. 147. Elsevier. ISSN: 2772-9508..
https://doi.org/10.1016/j.bioadv.2023.213328

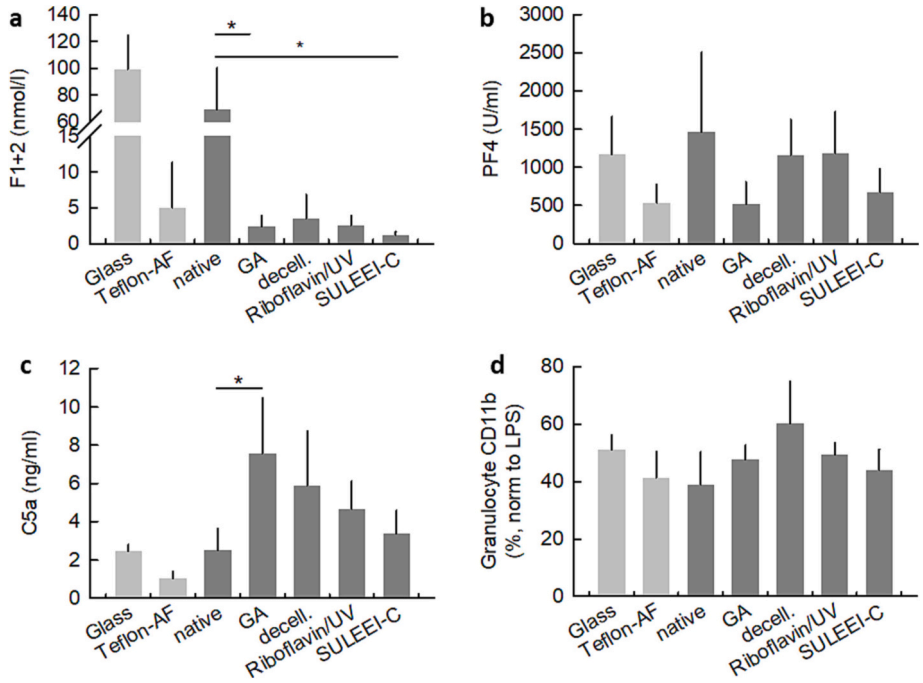

Fig. 7. Whole blood incubation of pericardium at different preparation steps of the SULEEI protocol (optimized modification C): native, glutaraldehyde fixed reference, decellularized sample, riboflavin/UV crosslinked samples and complete SULEEI-C protocol, including electron beam. Parameters as in Fig. 3. Data are presented as mean ± SD of n 6.

immunohistochemistry according to pericardia prepared with the SULEEI-A and B protocols. Native and decellularized pericardia exhibit a dense covering, positive for platelet marker CD61 and including CD15 positive granulocytes (Fig. 8). Granulocytes were stained in the inner part of the matrix at distances of 131.6 ± 69.7 μm from the blood incubated surface. This was significantly higher than in native or SULEEI-C treated pericardia with distances of 47.1 ± 26.4 μm and 59.3 ± 21.4 μm (4 sections of $n = 2$; Suppl. Fig. 3). The total count of invaded granulocytes was with 18.0 ± 12.7 mm ^{2} highest in decellularized pericardia compared to native and SULEEI-C pericardium (2.4 ± 2.0 mm ^{2} and 0.8 ± 0.6 mm ^{2}, respectively).

In order to evaluate the activation of the complement cascade on a histological level, the complement component C3 was stained using an antibody that detects C3, C3c and C3b by immunohistochemistry. A cover layer was intensively stained for C3 in native, decellularized and SULEEI samples on the blood-contacting serous side (Fig. 9a). GA-fixed pericardium showed the most intense signal not only on the blood-contacting surface (serous side) but also up to one third of the adjacent inner tissue matrix. Contrary, no staining was observed in the ECM at the surface without blood contact and respective inner ECM layers (Fig. 9a, b [respective magnifications of both serous and fibrous sides]). SULEEI-C pericardium exhibited a strong staining in the covering on the serous side after blood contact and a less intense background staining in collagen fibers in the entire tissue matrix (Fig. 9c).

3.4. SULEEI tissue properties and ECM

Testing of mechanical properties in uniaxial tensile tests revealed 42.0 ± 10.4 MPa for SULEEI-A, 31.2 ± 9.0 MPa for SULEEI-B and 32.5 ± 8.8 MPa for SULEEI-C, showing no significant changes of the Elastic Modulus in consequence to the protocol adaptation and also in comparison to native and GA-fixed pericardia (38.4 ± 3.0 MPa and 34.6 ± 15.3 MPa, respectively; $n \geq 5$; Fig. 10a). A significantly higher rate of degradability of all three SULEEI preparation was observed (SULEEI-A: remaining relative weight 59.0 ± 1.5 %; SULEEI-B 40.7 ± 5 % and C 51.9 ± 1.7 %) in in vitro collagen digestion assay compared to the native pericardium (66.4 ± 2.2 %). The GA-fixed counterpart was significantly more resistant with a remaining weight of 88.8 ± 3.7 % ($N = 8$ of $n = 3$; Fig. 10b). The calcification potential of SULEEI-C treated pericardium was lower (18d; 29.7 ± 8.9 μg calcium/mg dry weight in native tissue vs. 12.9 ± 4.3 μg/mg dry weight in SULEEI-C samples; n = 3) or comparable to native and GA-fixed samples (Fig. 10c).

Due to the possibility that the decellularization protocol might impact the pericardial ECM components, hydroxyproline and elastin content was determined and did not differ significantly between SULEEI-A to C (Suppl. Fig. 4a and b). Elastin content was in native tissue 47.8 ± 15.2 μg/mg dry weight and for SULEEI-A 46.0 ± 13.7 μg/mg dry weight. The more stringent decellularization in SULEEI-B and C resulted in values of 32.5 ± 19.5 and 32.0 ± 16.0 μg/mg dry weight, respectively. In contrast, differences were observed in the GAG content of the SULEEI treated material (A: 8.1 ± 1.7 μg/mg dry weight; B: 1.4 ± 0.4 μg/mg and C: 2.4 ± 0.4 μg/mg), independent from the protocol A-C, with lower values after trypsin containing protocols and compared to the native material (11.0 ± 2.6 μ/mg; Suppl. Fig. 4c; $N \geq 10$ of n = 3).

4. Discussion

The SULEEI-procedure is an innovative GA-free strategy to prepare pericardium for surgical applications. It combines decellularization and crosslinking of collagen matrix by UV-irradiation in riboflavin solution and irradiation with a low-energy-electron beam [38]. As the original SULEEI protocol was developed for thin porcine tissue, the protocol was adjusted here for the thicker bovine tissue, focusing on the hemocompatibility of the material in fresh human blood. The generally higher thickness of the bovine compared to porcine pericardium can affect the diffusion of the various bath solutions and UV and electron-beam penetration depth. Besides material thickness, preparation steps can be superposed by intra- and interindividual variation in tissue properties due to the range of age of the animals available for this study. Therefore, each set of samples for comparing the initial treatment protocols was prepared from the pericardium of each individual.

Optimization of the SULEEI protocol following the reactions of human whole blood provides a very targeted approach considering implants in the human vascular bed. Besides pre-selection and

Provided by Sächsische Landesbibliothek, Staats- und Universitätsbibliothek Dresden

Final edited version was published in Biomaterials advances. 2023. 147. Elsevier. ISSN: 2772-9508..
https://doi.org/10.1016/j.bioadv.2023.213328

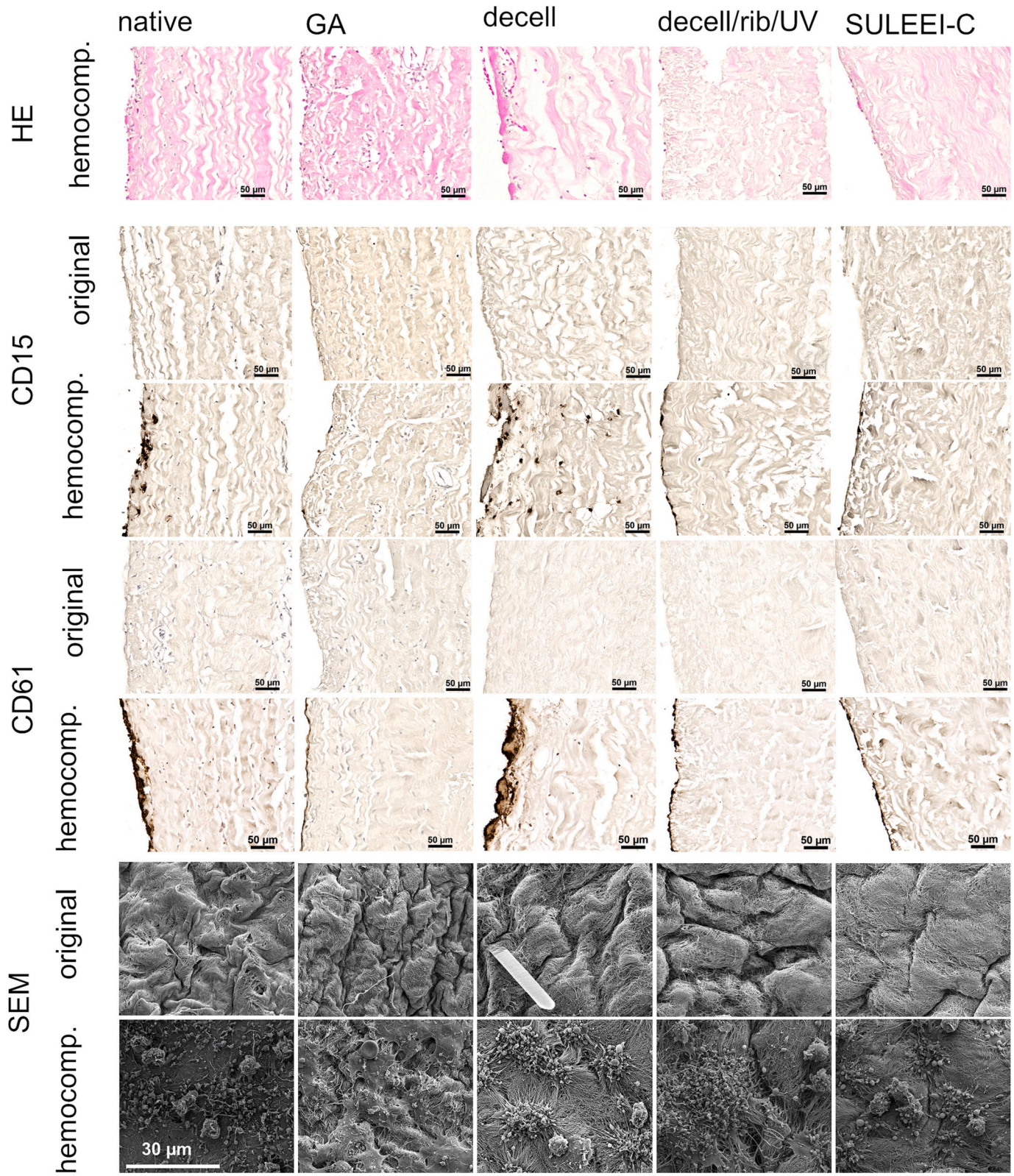

Fig. 8. Investigation of SULEEI-C treated pericardia and protocol intermediate tissues decellularized or additionally riboflavin/UV irradiated, after hemocompatibility incubation in comparison to native and GA-fixed and non-incubated (original) counterparts by immunohistochemistry and SEM. Dense fibrin covering on serous blood contacting side of native and merely decellularized pericardium is detected, containing CD15 positive granulocytes and CD61 positive platelets. Granulocytes were able to enter the inner collagen matrix of only decellularized material that exhibited a more permeable fiber density.

Provided by Sächsische Landesbibliothek, Staats- und Universitätsbibliothek Dresden

Final edited version was published in Biomaterials advances. 2023. 147. Elsevier. ISSN: 2772-9508..
https://doi.org/10.1016/j.bioadv.2023.213328

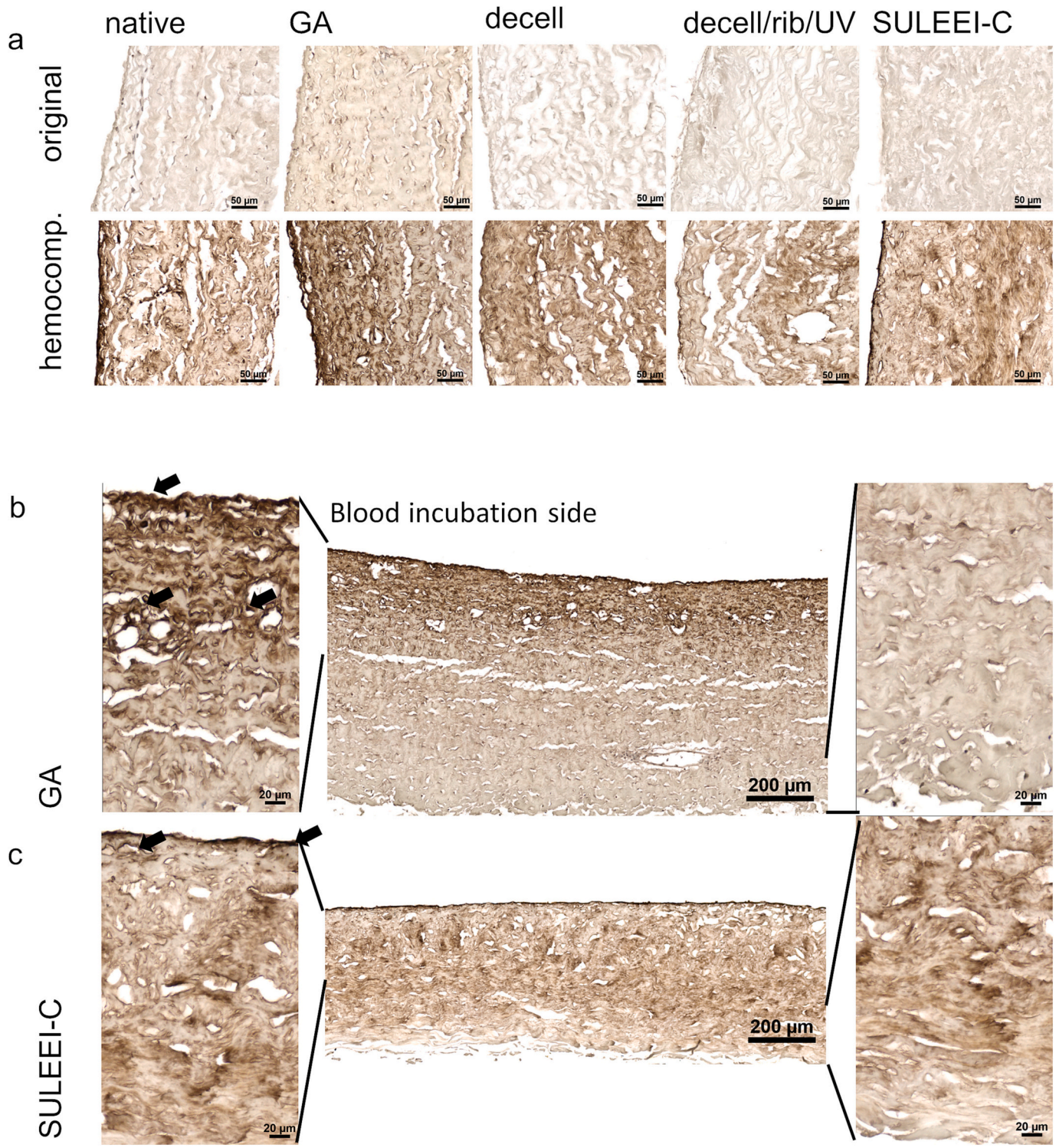

Fig. 9. Detection of complement component C3/C3b/C3c in native, GA-fixed and SULEEI-treated pericardia, including in intermediate protocol steps with and without blood incubation of the materials via immunohistochemistry. After GA-fixation, an intense staining signal is visible at the blood incubated surface and the adjacent matrix but not in the matrix of the non-contacting side.

restriction of subsequent animal implantation studies, because the incubation with human blood provides the unique opportunity to analyze additional aspects, such as complement activation due to xenogeneic epitopes, that would be missed in rodent implantation tests.

Two different protocols for the initial decellularization, including and excluding trypsin, were combined with two protocols for the riboflavin/UV-irradiation step with different riboflavin concentrations and UV intensities. Size limitations of the pericardium impeded the analysis of more systematic protocol combinations, but two protocols, SULEEI-A and SULEEI-B (Table 1), were selected and after a first evaluation round, the optimized protocol SULEEI-C was developed. The resulting materials were analyzed histologically and subjected to incubation in human whole blood to evaluate hemocompatibility.

GA fixed samples served as a reference in this study. The initial three-

Provided by Sächsische Landesbibliothek, Staats- und Universitätsbibliothek Dresden

Final edited version was published in Biomaterials advances. 2023. 147. Elsevier. ISSN: 2772-9508..
https://doi.org/10.1016/j.bioadv.2023.213328

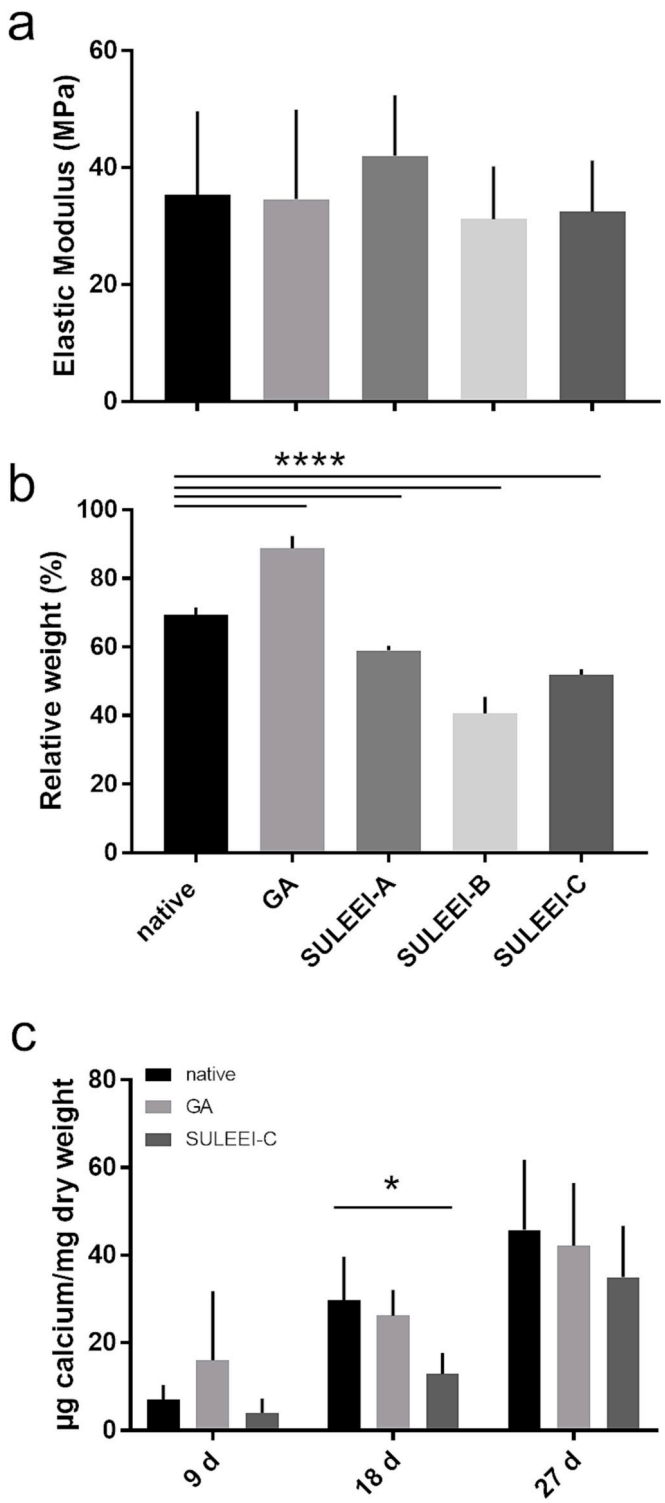

Fig. 10. Evaluation of material properties Elastic Modulus (a) in vitro degradability in enzymatic digestion (b) comparing SULEEI A, SULEEI-B and optimized SULEEI C pericardia vs. the native pericardium and GA-fixed counterparts. Calcium content (c) was determined after incubation of native, GA-fixed and SULEEI-C treated pericardia for up to 27 days in mSBF and related to tissue dry weight. a) One-way ANOVA, Tukey-Test; *p < 0.05; b) One-way ANOVA, Dunnett's multiple comparisons test, native pericardium as control; ***$p < 0.001$, ****p < 0.0001; c) One-way ANOVA, Tukey-Test; *p < 0.05 or n.s.

hour fixation step is part of an industrial protocol for the preparation of bovine aortic heart valve prostheses [51] and therefore was applied. In that published procedure, subsequent pericardial tissues were further incubated in GA for several weeks. Therefore the GA-fixed controls in the herein presented dataset, with a fixation time of merely 3 h, may be less efficiently cross-linked than commercial products, potentially presenting free aldehyde groups or containing adsorbed or depolymerized aldehyde causing cytotoxicity or reduced compatibility reactions [1,7,8,52,53]. Nevertheless, the degradability of the collagen matrix after GA-fixation was significantly reduced compared to the basic raw material.

Complement activation by GA-fixed vascular grafts has been described before [54,55], and GA-fixed cell membranes can activate complement on the classical pathway [56]. In this study, histological analysis of GA-fixed samples after hemocompatibility testing revealed C3/C3b/C3c epitopes, especially on the serosa surface of the GA-fixed pericardium but also penetrating the matrix adjacent to the blood-contacting surface. C3b is central in the complement system and initiator of the alternative pathway, where it is stabilized by binding to nucleophilic hydroxyl or amino groups and propagates the complement cascade further, resulting in an inflammatory response, e.g. increased adhesion of leukocytes [57–59]. It is reasonable to assume that residual reactive groups from GA fixation have similar C3b binding properties.

The protocol SULEEI-A used a mild initial decellularization step with DNase and RNase but without trypsin and only a short treatment time compared to SULEEI-B (Table 1). Indeed the glycosaminoglycan (GAG) content in SULEEI-A protocol was preserved best among the three protocols but still significantly lower than in native pericardium. GAGs have been identified as important for native AV function [60,61]. In porcine AV tissues GAGs impact cuspal thickness, water content and rehydration capacity; cyclic stress reduces the GAG content [62,63]. In vivo GA-fixed porcine AV tissues with additional GAG stabilization showed no advantage in the calcification potential and collagen/GAG stability [64]. It has to be substantiated for the SULEEI procedure if the natural GAG quantity of bovine pericardium is relevant for bioprostheses performance. Here, solely sulfated GAGs were determined, and the elastic moduli of SULEEI-B and C are comparable to the GA-fixed counterpart. Still, classification is necessary, which GAGs and proteoglycans actually impact bioprosthesis biomechanics and stability [65,66].

Besides the mechanical lubricant properties, GAGs have multiple biochemical functions that strongly depend on the individual type. Especially sulfated GAGs interact with multiple proteins and in this way stabilize growth factors [67]. Heparin and heparan sulfate catalyze the inhibition of coagulation factors by antithrombin III and heparin cofactor II and the inhibition of the inflammatory complement cascade by binding factor H. Mainly anti-inflammatory properties are ascribed to GAGs. The affinity of proinflammatory cytokines, such as IL-8, to GAGs can quench their concentration, however, also support leukocyte binding to GAG-IL-8 complex [68,69]. Although a high GAG content in the tissue appears desirable for the hemocompatibility of the tissue, it did not dominate the results of this study. Neither the GAG-rich native, GA fixed, nor SULEEI-A treated pericardia showed concordant results in coagulation or inflammation parameters, nor the GAG-poor SULEEI-B and SULEEI-C.

The milder decellularization protocol A resulted in DNA-residues and preservation of xenogeneic epitopes such as α-Gal, detected histologically in the matrix of SULEEI-A treated pericardia (Fig. 2). The more stringent decellularization protocol in SULEEI-B, including trypsin to access the interstitial cells and inner pericardial vessel structures, led to reduced values for remaining DNA and α-Gal epitopes, and also to lower coagulation activation (F1 + 2 in Fig. 4a and fibrin network in the SEM images Fig. 5). The control of thrombogenicity did benefit more from this stringent decellularization than the inflammation control, which did respond more to the differences in the riboflavin/UV crosslinking step, performed under stronger conditions in the protocol SULEEI-A than SULEEI-B.

Provided by Sächsische Landesbibliothek, Staats- und Universitätsbibliothek Dresden

Final edited version was published in Biomaterials advances. 2023. 147. Elsevier. ISSN: 2772-9508..
https://doi.org/10.1016/j.bioadv.2023.213328

Based on the observed requirement of sufficient decellularization to induce a low hemostatic response and an efficient riboflavin/UV crosslinking step to obtain a low inflammatory response, the protocol SULEEI-C was developed. Nucleophilic groups, such as hydroxyl groups stabilize spontaneously formed C3b fragments on the surface and propagate the complement cascade on the alternative pathway [70]; a similar effect can be expected for non-saturated radicals. The hydroxyl groups of the polysaccharide dextran and the high riboflavin concentration in the UV crosslinking step of SULEEI-A, therefore, were assumed to cause reactive sites for complement activation, although it was not prominent for the high dextran (SULEEI-A) but for the high riboflavin (SULEEI-B) protocol (Fig. 4). In consequence, the lower riboflavin concentration was applied, and dextran as bulking molecule was skipped entirely in the final protocol. Analysis of blood activation reactions in intermediate steps of the SULEEI-C protocol, along with the results of the SULEEI-A and B samples, allows conclusions on activation mechanisms.

Residual tissue factor was assumed to be responsible for the high coagulation in the native and the SULEEI-A samples on the extrinsic pathway. The high coagulation activation by the SULEEI-A treated tissue indicates that the riboflavin/UV crosslinking and electron beam treatment steps of the SULEEI process were not sufficient to inactivate the biological activity of ECM proteins. The mild decellularization step increased the coagulation, even exceeding the values of the native pericardium, due to better accessibility of the tissue for the coagulation system.

The UV treatment on riboflavin-incubated pericardia induced free radicals and caused oxidative crosslinking of proteins [39], substituting the GA crosslinking in the SULEEI protocols. While the crosslinking step with riboflavin/UV is capable of inactivating proteins by oxidation, it also leads to the formation of procoagulant free radicals [71]. Electron irradiation can quench free radicals and also denature proteins, leading to further reduced coagulation, as seen in Fig. 7a. Both steps tended to decrease the procoagulant effects of the tissue (Fig. 7a), but efficient decellularization, including trypsin, had the highest inactivating effect (SULEEI-B and SULEEI-C). The crosslinking steps of SULEEI were not as efficient as GA in inactivating tissue factor.

The GA-fixation process has been described to inactivate the α-Gal only incompletely [22,72], and the role of this epitope (as well as other xenogeneic epitopes) for prosthesis deterioration years after implantation is not clearly discovered [73–75]. Therefore, α-Gal still might impact long-term biological response. Comparison of SULEEI-A and SULEEI-B showed, that the more aggressive, trypsin-containing decellularization step of SULEEI-B was necessary to remove the α-Gal epitope. Human plasma contains high concentrations of preformed α-Gal antibodies type IgM and IgG, mainly resulting from the enterobacteria of the intestinal flora and leading to immune protection against enterobacteria pathogen but also as a result of a tick bite [58,76]. Due to structural similarities of the blood group antigens A and B with the α-Gal antigen, patients with this blood group tolerate xenografts better than patients with blood group O [47,77]. For enhanced sensitivity, the study was performed with blood of blood group O.

Previous blood incubation tests with allogenic and xenogenic cell cultures showed elevated complement activation for the xenogenic cells, which was attributed to the α-Gal epitope [78]. Therefore, elevated complement activation on the classical pathway was expected due to anti-α-Gal antibodies; however, the C5a fragment concentrations (Fig. 4c) did not correlate with the α-Gal presentation of the samples (Fig. 2b). Various reasons can be assumed: The complement cascade might be interrupted before C5 cleavage, e.g. by physiological inhibitors Factor H or C4b binding protein. α-Gal-independent activation in SULEEI-B may be attributed to alternative pathway activation at hydroxyl groups of the polysaccharide dextran and C3b binding to reactive groups obtained by the aggressive crosslinking step [57]. The crosslinking-protocol in SULEEI-C with low riboflavin concentration and without dextran caused only low complement activation, confirming the strategy.

The trypsin treatment was necessary to remove tissue factor and the xeno-antigen α-Gal from the tissue. However, it may contribute to the elevated complement activation in SULEEI-B, in addition to the high riboflavin/dextran treatment. Also, residual trypsin activity is capable of activating various steps of the complement cascade [79]. The subsequent riboflavin/UV crosslinking and electron beam treatment appear necessary to sufficiently inactivate the enzyme.

Histologic analysis showed loose fiber structure and a low density of the decellularized and still in the riboflavin/UV crosslinked samples, different from native and from final SULEEI-treated tissues. Immunohistological detection of granulocytes (CD15) indicated a higher penetration of cells. This increased accessibility to the ECM can be a reason for the reduced hemocompatibility detected in flow cytometry after incubation with the decellularized tissue. Subsequent collagen crosslinking protocol steps effectively prevented granulocyte penetration.

C5a is among the strongest activators of leukocytes. The CD11b expression on granulocytes as activation-marker was higher for the SULEEI fixed samples than for native or GA fixed samples (Fig. 4d). Additional, non-identified activation processes of the leukocytes may play a role. SULEEI-A caused higher loss of granulocytes from the blood than SULEEI-B (Suppl. Fig. 1). Probably, this loss of cells due to adhesion and penetration into the surface mainly affected highly activated cells and, therefore, the CD11b level of the remaining cells in the blood was lower.

Adaptation of the SULEEI-process for more effective decellularization and a less activating riboflavin/UV crosslinking step (SULEEI-C) resulted in a better hemocompatibility of the tissue. However, the effect on basic structural and mechanical properties had to be actualized. The comparable elastic moduli in the SULEEI-C sample confirmed that mechanical properties are comparable to the native and GA-control. But for all SULEEI pericardia, a higher degradability than in the GA-fixed samples was detected, independent of the SULEEI protocol refinement. Higher enzymatic degradability of SULEEI-pericardium in this laboratory setup is described before [15,38] but due to the enzyme concentration does not reflect an in vivo situation. Increased accessibility can rather be advantageous, especially regarding remodeling processes [15,80]. Hydroxyproline and elastin content of the tissues resulting from SULEEI-A, B or C did not differ significantly. A high variability in elastin content of the tissue segments examined according to the individual pericardia was detected in general and depended on the individual tissue segment. The in vitro calcification potential did not differ between the final SULEEI-C protocol and GA-fixed counterparts, further supporting SULEEI-C protocol applicability as a pretreatment strategy.

The in vitro incubations with human whole blood allowed for more rapid and flexible process optimization and elaboration of the SULEEI-C protocol than any animal study would do. While unnecessary animal experiments were avoided during these optimization loops, tissue processed according to the SULEEI-C protocol can now be confidentially tested for biocompatibility in animals as subsequent studies. Relevant tests would be thrombogenicity tests in a perfusion experiment, such as an arteriovenous shunt model [81,82]. Further, a rat subcutaneous implantation study, supplemented by in vitro cell culture tests, is ongoing in our study group to provide more information about the long-term inflammatory response and degradation and more valid information about calcification. Upon favorable results, the analysis of the optimized SULEEI-C treated material in the geometry of real valves in vitro and in large animal models in aortic valve position is envisioned [81–84]. Basis for GA-free preparation strategies such as the SULEEI-protocol can also be α-Gal knock out tissues as designed for xeno-transplantation [85].

5. Conclusion

Using hemocompatibility testing the glutaraldehyde-free SULEEI-protocol to fix bovine pericardium for surgical application was optimized for low hemostatic and inflammatory reactions. Improved final protocol combines an intense, trypsin-containing decellularization step

Provided by Sächsische Landesbibliothek, Staats- und Universitätsbibliothek Dresden

Final edited version was published in Biomaterials advances. 2023. 147. Elsevier. ISSN: 2772-9508..
https://doi.org/10.1016/j.bioadv.2023.213328

to inactivate tissue factor with a dextran-free low riboflavin/high UV crosslinking step, followed by low energy electron beam irradiation (SULEEI). The resulting improved SULEEI – procedure for bovine pericardium preparation is a promising GA-free alternative intensely validated in hemocompatibility with human blood in this study to be further justified in in vivo tests.

Supplementary data to this article can be found online at https://doi.org/10.1016/j.bioadv.2023.213328.

CRediT authorship contribution statement

Conceptualization: CD, MM; Methodology: MM, CD, CS, UK; Formal analysis and investigation: MM, CD, CW, EB, SB; Writing - original draft preparation: CD, MM; Writing - review and editing: MM, CS, SMT, AJ, UK, KA; Funding acquisition: SMT, CD, UK, AJ; Supervision: SMT, MM, CD.

Funding and acknowledgements

This project is funded by the European Regional Development Fund (EFRE) and the Free State of Saxony (Number: 100367226). The excellent technical assistance of Jennifer Mittag, Lysann Kenner, Stefanie Hänsel, Maria Feilmeier and Dominic Salminger is acknowledged.

Histological images were acquired and processed using equipment of the Biopolis Dresden Imaging Platform at the BIOTEC/CRTD–Light Microscopy Facility and the MTZ-Core Facility Cellular Imaging.

Declaration of competing interest

The authors have no relevant financial or non-financial interests to disclose. The authors have no competing interests to declare that are relevant to the content of this article.

Data availability

Data will be made available on request.

References

[1] E.A. Grebenik, E.R. Gafarova, L.P. Istranov, E.V. Istranova, X. Ma, J. Xu, W. Guo, A. Atala, P.S. Timashev, Mammalian pericardium-based bioprosthetic materials in xenotransplantation and tissue engineering, Biotechnol. J. 15 (8) (2020), e1900334.

[2] L. Iop, T. Palmosi, E. Dal Sasso, G. Gerosa, Bioengineered tissue solutions for repair, correction and reconstruction in cardiovascular surgery, J. Thorac. Dis. 10 (Suppl 20) (2018) S2390–S2411.

[3] L. Grefen, F. Konig, M. Grab, C. Hagl, N. Thierfelder, Pericardial tissue for cardiovascular application: an in-vitro evaluation of established and advanced production processes, J Mater Sci Mater Med 29 (11) (2018) 172.

[4] A.E. Kostyunin, A.E. Yuzhalin, M.A. Rezvova, E.A. Ovcharenko, T.V. Glushkova, A. G. Kutikhin, Degeneration of bioprosthetic heart valves: update 2020, J. Am. Heart Assoc. 9 (19) (2020), e018506.

[5] D. Dvir, T. Bourguignon, C.M. Otto, R.T. Hahn, R. Rosenhek, J.G. Webb, H. Treede, M.E. Sarano, T. Feldman, H.C. Wijeysundera, Y. Topilsky, M. Aupart, M.J. Reardon, G.B. Mackensen, W.Y. Szeto, R. Kornowski, J.S. Gammie, A.P. Yoganathan, Y. Arbel, M.A. Borger, M. Simonato, M. Reisman, R.R. Makkar, A. Abizaid, J. M. McCabe, G. Dahle, G.S. Aldea, J. Leipsic, P. Pibarot, N.E. Moat, M.J. Mack, A. P. Kappetein, M.B. Leon, V. Investigators, Standardized definition of structural valve degeneration for surgical and transcatheter bioprosthetic aortic valves, Circulation 137 (4) (2018) 388–399.

[6] A.G. Fiedler, G. Tolis Jr., Surgical treatment of valvular heart disease: overview of mechanical and tissue prostheses, advantages, disadvantages, and implications for clinical use, Curr. Treat. Opt. Cardiovasc. Med. 20 (1) (2018) 7.

[7] H.J. Kim, J.W. Bae, C.H. Kim, J.W. Lee, J.W. Shin, K.D. Park, Acellular matrix of bovine pericardium bound with L-arginine, Biomed. Mater. 2 (3) (2007) S111–S116.

[8] H.W. Chang, S.H. Kim, K.H. Kim, Y.J. Kim, Combined anti-calcification treatment of bovine pericardium with amino compounds and solvents, Interact. Cardiovasc. Thorac. Surg. 12 (6) (2011) 903–907.

[9] C.W. Baird, P.O. Myers, B. Piekarski, M. Borisuk, A. Majeed, S.M. Emani, S. P. Sanders, M. Nathan, P.J. Del Nido, Photo-oxidized bovine pericardium in congenital cardiac surgery: single-centre experience, Interact. Cardiovasc. Thorac. Surg. 24 (2) (2017) 240–244.

[10] S.P. Marathe, M. Chavez, L.A. Sleeper, G.R. Marx, K. Friedman, E.N. Feins, P.J. Del Nido, C.W. Baird, Single-leaflet aortic valve reconstruction utilizing the Ozaki technique in patients with congenital aortic valve disease, Semin. Thorac. Cardiovasc. Surg. 34 (4) (2022) 1262–1272.

[11] W.M.L. Neethling, K. Puls, A. Rea, Comparison of physical and biological properties of CardioCel (R) with commonly used bioscaffolds, Interact. Cardiovasc. Thorac. Surg. 26 (6) (2018) 985–992.

[12] X.K. Qi, Z.L. Jiang, M.Z. Song, Z.J. Tang, X.L. Xie, Y.H. Liu, Q.Y. Wu, Z.S. Wu, A novel crosslinking method for improving the anti-calcification ability and extracellular matrix stability in transcatheter heart valves, Front. Bioeng. Biotechnol. 10 (2022).

[13] Y. Luo, S.Y. Huang, L. Ma, A novel detergent-based decellularization combined with carbodiimide crosslinking for improving anti-calcification of bioprosthetic heart valve, Biomed. Mater. 16 (4) (2021).

[14] F. Yang, L.P. Xu, G.Y. Guo, Y.B. Wang, Visible light-induced cross-linking of porcine pericardium for the improvement of endothelialization, anti-tearing, and anticalcification properties, J. Biomed. Mater. Res. A 110 (1) (2022) 31–42.

[15] S. Walker, C. Dittfeld, A. Jakob, J. Schonfelder, U. Konig, S.M. Tugtekin, Sterilization and cross-linking combined with ultraviolet irradiation and low-energy electron irradiation procedure: new perspectives for bovine pericardial implants in cardiac surgery, Thorac. Cardiovasc. Surg. 70 (1) (2022) 33–42.

[16] Y. Lei, G. Guo, W. Jin, M. Liu, Y. Wang, Riboflavin photo-cross-linking method for improving elastin stability and reducing calcification in bioprosthetic heart valves, Xenotransplantation 26 (2) (2019), e12481.

[17] S. Nordmeyer, P. Murin, A. Schulz, F. Danne, J. Nordmeyer, J. Kretzschmar, D. Sumbadze, K.R.L. Schmitt, O. Miera, M.Y. Cho, N. Sinzobahamvya, F. Berger, S. Ovroutski, J. Photiadis, Results of aortic valve repair using decellularized bovine pericardium in congenital surgery, Eur. J. Cardio-Thorac. 54 (6) (2018) 986–992.

[18] O. Deutsch, F. Bruehl, J. Cleuziou, A. Prinzing, A.M. Schlitter, M. Krane, R. Lange, Histological examination of explanted tissue-engineered bovine pericardium following heart valve repair, Interact. Cardiovasc. Thorac. Surg. 30 (1) (2020) 64–73.

[19] S.C. Chivers, C. Pavy, R. Vaja, C. Quarto, O. Ghez, P.E.F. Daubeney, The ozaki procedure with CardioCel patch for children and young adults with aortic valve disease: preliminary experience - a word of caution, World J. Pediatr. Cong. 10 (6) (2019) 724–730.

[20] P. Simon, M.T. Kasimir, G. Seebacher, G. Weigel, R. Ullrich, U. Salzer-Muhar, E. Rieder, E. Wolner, Early failure of the tissue engineered porcine heart valve SYNERGRAFT in pediatric patients, Eur J Cardiothorac Surg 23 (6) (2003) 1002–1006, discussion 1006.

[21] M. Meyer, Processing of collagen based biomaterials and the resulting materials properties, Biomed. Eng. Online 18 (1) (2019) 24.

[22] F. Naso, A. Gandaglia, T. Bottio, V. Tarzia, M.B. Nottle, A.J.F. d'Apice, P.J. Cowan, E. Cozzi, C. Galli, I. Lagutina, G. Lazzari, L. Iop, M. Spina, G. Gerosa, First quantification of alpha-gal epitope in current glutaraldehyde-fixed heart valve bioprostheses, Xenotransplantation 20 (4) (2013) 252–261.

[23] F. Naso, A. Gandaglia, L. Iop, M. Spina, G. Gerosa, Alpha-gal detectors in xenotransplantation research: a word of caution, Xenotransplantation 19 (4) (2012) 215–220.

[24] U. Galili, Interaction of the natural anti-gal antibody with alpha-galactosyl epitopes: a major obstacle for xenotransplantation in humans, Immunol. Today 14 (10) (1993) 480–482.

[25] P.M. Crapo, T.W. Gilbert, S.F. Badylak, An overview of tissue and whole organ decellularization processes, Biomaterials 32 (12) (2011) 3233–3243.

[26] F. Naso, A. Gandaglia, Different approaches to heart valve decellularization: a comprehensive overview of the past 30 years, Xenotransplantation 25 (1) (2018).

[27] R. Ramm, T. Goecke, K. Theodoridis, K. Hoeffler, S. Sarikouch, K. Findeisen, A. Ciubotaru, S. Cebotari, I. Tudorache, A. Haverich, A. Hilfiker, Decellularization combined with enzymatic removal of N-linked glycans and residual DNA reduces inflammatory response and improves performance of porcine xenogeneic pulmonary heart valves in an ovine in vivo model, Xenotransplantation 27 (2) (2020), e12571.

[28] P. Iablonskii, S. Cebotari, A. Ciubotaru, S. Sarikouch, K. Hoeffler, A. Hilfiker, A. Haverich, I. Tudorache, Decellularized mitral valve in a long-term sheep model, Eur. J. Cardiothorac. Surg. 53 (6) (2018) 1165–1172.

[29] K. Findeisen, L. Morticelli, T. Goecke, L. Kolbeck, R. Ramm, H.K. Hoffler, G. Brandes, S. Korossis, A. Haverich, A. Hilfiker, Toward acellular xenogeneic heart valve prostheses: histological and biomechanical characterization of decellularized and enzymatically deglycosylated porcine pulmonary heart valve matrices, Xenotransplantation 27 (5) (2020), e12617.

[30] U. Galili, Anti-gal: an abundant human natural antibody of multiple pathogeneses and clinical benefits, Immunology 140 (1) (2013) 1–11.

[31] T. Senage, A. Paul, T. Le Tourneau, I. Fellah-Hebia, M. Vadori, S. Bashir, M. Galinanes, T. Bottio, G. Gerosa, A. Evangelista, L.P. Badano, A. Nassi, C. Costa, G. Cesare, R.A. Manji, C. Cueff de Monchy, N. Piriou, R. Capoulade, J.M. Serfaty, G. Guimbretiere, E. Dantan, A. Ruiz-Majoral, G. Coste du Fou, S. Leviatan Ben-Arye, L. Govani, S. Yehuda, S. Bachar Abramovitch, R. Amon, E.M. Reuven, Y. Atiya-Nasagi, H. Yu, L. Iop, K. Casos, S.G. Kuguel, A. Blasco-Lucas, E. Permanyer, F. Sbraga, R. Llatjos, G. Moreno-Gonzalez, M. Sanchez-Martinez, M. E. Breimer, J. Holgersson, S. Teneberg, M. Pascual-Gilabert, A. Nonell-Canals, Y. Takeuchi, X. Chen, R. Manez, J.C. Roussel, J.P. Soulillou, E. Cozzi, V. Padler-Karavani, The role of antibody responses against glycans in bioprosthetic heart valve calcification and deterioration, Nat. Med. 28 (2) (2022) 283–294.

[32] S.L. Blok, G.E. Engels, W. van Oeveren, In vitro hemocompatibility testing: the importance of fresh blood, Biointerphases 11 (2) (2016), 029802.

Provided by Sächsische Landesbibliothek, Staats- und Universitätsbibliothek Dresden

Final edited version was published in Biomaterials advances. 2023. 147. Elsevier. ISSN: 2772-9508..
https://doi.org/10.1016/j.bioadv.2023.213328

[33] M. Weber, H. Steinle, S. Golombek, L. Hann, C. Schlensak, H.P. Wendel, M. Avci-Adali, Blood-contacting biomaterials: in vitro evaluation of the hemocompatibility, Front. Bioeng. Biotechnol. 6 (2018) 99.
[34] M. Ground, S. Waqanivavalagi, R. Walker, P. Milsom, J. Cornish, Models of immunogenicity in preclinical assessment of tissue engineered heart valves, Acta Biomater. 133 (2021) 102–113.
[35] U. Streller, C. Sperling, J. Hubner, R. Hanke, C. Werner, Design and evaluation of novel blood incubation systems for in vitro hemocompatibility assessment of planar solid surfaces, J. Biomed. Mater. Res. B Appl. Biomater. 66 (1) (2003) 379–390.
[36] C. Sperling, M.F. Maitz, C. Werner, Test Methods for Hemocompatibility of Biomaterials, 2018.
[37] M.F. Maitz, C. Sperling, T. Wongpinyochit, M. Herklotz, C. Werner, F.P. Seib, Biocompatibility assessment of silk nanoparticles: hemocompatibility and internalization by human blood cells, Nanomed.Nanotechnol. 13 (8) (2017) 2633–2642.
[38] S. Walker, J. Schonfelder, S.M. Tugtekin, C. Wetzel, M.C. Hacker, M. Schulz-Siegmund, Stabilization and sterilization of pericardial scaffolds by ultraviolet and low-energy electron irradiation, Tissue Eng Part C Methods 24 (12) (2018) 717–729.
[39] Y. Kang, J.H. Kim, S.Y. Kim, W.G. Koh, H.J. Lee, Blue light-activated riboflavin phosphate promotes collagen crosslinking to modify the properties of connective tissues, Materials (Basel) 14 (19) (2021).
[40] G. Wollensak, E. Spoerl, T. Seiler, Riboflavin/ultraviolet-A-induced collagen crosslinking for the treatment of keratoconus, Am J. Ophthalmol. 135 (5) (2003) 620–627.
[41] F. Raiskup, E. Spoerl, Corneal crosslinking with riboflavin and ultraviolet A. I. Principles, Ocul. Surf. 11 (2) (2013) 65–74.
[42] D. Wu, D.K. Lim, B.X.H. Lim, N. Wong, F. Hafezi, R. Manotosh, C.H.L. Lim, Corneal cross-linking: the evolution of treatment for corneal diseases, Front. Pharmacol. 12 (2021), 686630.
[43] M.R. Santhiago, J.B. Randleman, The biology of corneal cross-linking derived from ultraviolet light and riboflavin, Exp. Eye Res. 202 (2021), 108355.
[44] K.H. Schneider, S. Rohringer, B. Kapeller, C. Grasl, H. Kiss, S. Heber, I. Walter, A. H. Teuschl, B.K. Podesser, H. Bergmeister, Riboflavin-mediated photooxidation to improve the characteristics of decellularized human arterial small diameter vascular grafts, Acta Biomater. 116 (2020) 246–258.
[45] T.G. Seiler, M.A. Komninou, M.H. Nambiar, K. Schuerch, B.E. Frueh, P. Buchler, Oxygen kinetics during corneal cross-linking with and without supplementary oxygen, Am J. Ophthalmol. 223 (2021) 368–376.
[46] A. Roosens, P. Somers, F. De Somer, V. Carriel, G. Van Nooten, R. Cornelissen, Impact of detergent-based decellularization methods on porcine tissues for heart valve engineering, Ann. Biomed. Eng. 44 (9) (2016) 2827–2839.
[47] J.S. Manji, R.V. Rajotte, A. Koshal, R.A. Manji, Human anti-a and anti-B antibodies interact with anti-alpha gal antibody affecting xenograft survival, Xenotransplantation 11 (4) (2004) 376–377.
[48] L.B. Creemers, D.C. Jansen, A. vanVeenReurings, V. Everts, T. vandenBos, Microassay for the assessment of low levels of hydroxyproline, Biotechniques 22 (4) (1997) 656–658.
[49] T. Kokubo, H. Takadama, How useful is SBF in predicting in vivo bone bioactivity? Biomaterials 27 (15) (2006) 2907–2915.
[50] A. Oyane, H.M. Kim, T. Furuya, T. Kokubo, T. Miyazaki, T. Nakamura, Preparation and assessment of revised simulated body fluids, J. Biomed. Mater. Res. A 65a (2) (2003) 188–195.
[51] C.A.F. Carpentier, S.M. Patent, Methods for Treating Mplantable Biological Tissues to Mitigate the Calcification Thereof and Boprosthetic Articles Treated by Such Methods, 2003.
[52] C. Lee, H.G. Lim, C.H. Lee, Y.J. Kim, Effects of glutaraldehyde concentration and fixation time on material characteristics and calcification of bovine pericardium: implications for the optimal method of fixation of autologous pericardium used for cardiovascular surgery, Interact. Cardiovasc. Thorac. Surg. 24 (3) (2017) 402–406.
[53] P. Human, D. Bezuidenhout, E. Aikawa, P. Zilla, Residual bioprosthetic valve immunogenicity: forgotten, not lost, Front. Cardiovasc. Med. 8 (2021) 760635.
[54] E.Y. Wang, P.C. Giclas, R.H. Tu, C. Hata, R.C. Quijano, A comparative study of complement activation by Denaflex, Bioflow, and BioPolyMeric vascular grafts, ASAIO J 39 (3) (1993) M691–M694.
[55] P. Aguiari, L. Iop, F. Favaretto, C.M. Fidalgo, F. Naso, G. Milan, V. Vindigni, M. Spina, F. Bassetto, A. Bagno, R. Vettor, G. Gerosa, In vitro comparative assessment of decellularized bovine pericardial patches and commercial bioprosthetic heart valves, Biomed. Mater. 12 (1) (2017), 015021.
[56] N.C. Hughesjones, B. Gardner, J. Rowlands, Activation of human complement by glutaraldehyde-treated red-cells, Nature 270 (5638) (1977) 613–614.
[57] C. Sperling, M.F. Maitz, S. Talkenberger, M.F. Gouzy, T. Groth, C. Werner, In vitro blood reactivity to hydroxylated and non-hydroxylated polymer surfaces, Biomaterials 28 (25) (2007) 3617–3625.
[58] S.J. Bozso, R. El-Andari, D. Al-Adra, M.C. Moon, D.H. Freed, J. Nagendran, J. Nagendran, A review of the immune response stimulated by xenogenic tissue heart valves, Scand. J. Immunol. 93 (4) (2021), e13018.
[59] M. Vadori, E. Cozzi, The immunological barriers to xenotransplantation, Tissue Antigens 86 (4) (2015) 239–253.
[60] R.M. Buchanan, M.S. Sacks, Interlayer micromechanics of the aortic heart valve leaflet, Biomech Model Mechan 13 (4) (2014) 813–826.
[61] A.M. Porras, J.A. Westlund, A.D. Evans, K.S. Masters, Creation of disease-inspired biomaterial environments to mimic pathological events in early calcific aortic valve disease, Proc. Natl. Acad. Sci. U. S. A. 115 (3) (2018) E363–E371.
[62] N. Vyavahare, M. Ogle, F.J. Schoen, R. Zand, D.C. Gloeckner, M. Sacks, R.J. Levy, Mechanisms of bioprosthetic heart valve failure: fatigue causes collagen denaturation and glycosaminoglycan loss, J. Biomed. Mater. Res. 46 (1) (1999) 44–50.
[63] J.J. Lovekamp, D.T. Simionescu, J.J. Mercuri, B. Zubiate, M.S. Sacks, N. R. Vyavahare, Stability and function of glycosaminoglycans in porcine bioprosthetic heart valves, Biomaterials 27 (8) (2006) 1507–1518.
[64] J.J. Mercuri, J.J. Lovekamp, D.T. Simionescu, N.R. Vyavahare, Glycosaminoglycan-targeted fixation for improved bioprosthetic heart valve stabilization, Biomaterials 28 (3) (2007) 496–503.
[65] A. Cigliano, A. Gandaglia, A.J. Lepedda, E. Zinellu, F. Naso, A. Gastaldello, P. Aguiari, P. De Muro, G. Gerosa, M. Spina, M. Formato, Fine structure of glycosaminoglycans from fresh and decellularized porcine cardiac valves and pericardium, Biochem. Res. Int. 2012 (2012), 979351.
[66] B. Mendoza-Novelo, E.E. Avila, J.V. Cauich-Rodriguez, E. Jorge-Herrero, F.J. Rojo, G.V. Guinea, J.L. Mata-Mata, Decellularization of pericardial tissue and its impact on tensile viscoelasticity and glycosaminoglycan content, Acta Biomater. 7 (3) (2011) 1241–1248.
[67] H. Hutchings, N. Ortega, J. Plouet, Extracellular matrix-bound vascular endothelial growth factor promotes endothelial cell adhesion, migration, and survival through integrin ligation, FASEB J. 17 (11) (2003) 1520–1522.
[68] N. Lohmann, L. Schirmer, P. Atallah, E. Wandel, R.A. Ferrer, C. Werner, J.C. Simon, S. Franz, U. Freudenberg, Glycosaminoglycan-based hydrogels capture inflammatory chemokines and rescue defective wound healing in mice, Sci. Transl. Med. 9 (386) (2017).
[69] S. Morla, Glycosaminoglycans and glycosaminoglycan mimetics in cancer and inflammation, Int. J. Mol. Sci. 20 (8) (2019).
[70] M. Gorbet, C. Sperling, M.F. Maitz, C.A. Siedlecki, C. Werner, M.V. Sefton, The blood compatibility challenge. Part 3: material associated activation of blood cascades and cells, Acta Biomater. 94 (2019) 25–32.
[71] D.R. Crabtree, D. Muggeridge, S.J. Leslie, I.L. Megson, J.N. Cobley, To clot or not to clot? That is a free radical question, J Physiol 596 (20) (2018) 4805–4806.
[72] K.Z. Konakci, B. Bohle, R. Blumer, W. Hoetzenecker, G. Roth, B. Moser, G. Boltz-Nitulescu, M. Gorlitzer, W. Klepetko, E. Wolner, H.J. Ankersmit, Alpha-gal on bioprostheses: xenograft immune response in cardiac surgery, Eur. J. Clin. Investig. 35 (1) (2005) 17–23.
[73] A. Mangold, T. Szerafin, K. Hoetzenecker, S. Hacker, M. Lichtenauer, T. Niederpold, S. Nickl, M. Dworschak, R. Blumer, J. Auer, H.J. Ankersmit, Alpha-gal specific IgG immune response after implantation of bioprostheses, Thorac. Cardiovasc. Surg. 57 (4) (2009) 191–195.
[74] C.S. Park, S.S. Oh, Y.E. Kim, S.Y. Choi, H.G. Lim, H. Ahn, Y.J. Kim, Anti-alpha-gal antibody response following xenogeneic heart valve implantation in adults, J. Heart Valve Dis. 22 (2) (2013) 222–229.
[75] S. Mathapati, R.S. Verma, K.M. Cherian, S. Guhathakurta, Inflammatory responses of tissue-engineered xenografts in a clinical scenario, Interact. Cardiovasc. Thorac. Surg. 12 (3) (2011) 360–365.
[76] A.M. Calafiore, A. Haverich, M. Gaudino, M. Di Mauro, K. Fattouch, S. Prapas, P. Zilla, Immunoreaction to xenogenic tissue in cardiac surgery: alpha-gal and beyond, Eur. J. Cardiothorac. Surg. 62 (1) (2022), ezac115.
[77] O. Schussler, N. Lila, T. Perneger, P. Mootoosamy, J. Grau, A. Francois, D. M. Smadja, Y. Lecarpentier, M. Ruel, A. Carpentier, Recipients with blood group a associated with longer survival rates in cardiac valvular bioprostheses, EBioMedicine 42 (2019) 54–63.
[78] M. Herklotz, J. Hanke, S. Hansel, J. Drichel, M. Marx, M.F. Maitz, C. Werner, Biomaterials trigger endothelial cell activation when co-incubated with human whole blood, Biomaterials 104 (2016) 258–268.
[79] M. Huber-Lang, K.N. Ekdahl, R. Wiegner, K. Fromell, B. Nilsson, Auxiliary activation of the complement system and its importance for the pathophysiology of clinical conditions, Semin. Immunopathol. 40 (1) (2018) 87–102.
[80] F. Li, W. Li, S. Johnson, D. Ingram, M. Yoder, S. Badylak, Low-molecular-weight peptides derived from extracellular matrix as chemoattractants for primary endothelial cells, Endothelium 11 (3–4) (2004) 199–206.
[81] Y. Yang, P. Gao, J. Wang, Q. Tu, L. Bai, K. Xiong, H. Qiu, X. Zhao, M.F. Maitz, H. Wang, X. Li, Q. Zhao, Y. Xiao, N. Huang, Z. Yang, Endothelium-mimicking multifunctional coating modified cardiovascular stents via a stepwise metal-catechol-(Amine) surface engineering strategy, Research. (Wash. D. C.) 2020 (2020) 9203906.
[82] X.Y. Liang, C. Zheng, K.L. Ding, X.Y. Huang, S.M. Zhang, Y. Lei, K. Yu, Y.B. Wang, Arginine-grafted porcine pericardium by copolymerization to improve the cytocompatibility, hemocompatibility and anti-calcification properties of bioprosthetic heart valve materials, J. Mater. Chem. B 10 (29) (2022) 5571–5581.
[83] K. Ren, W.X. Duan, Z.W. Liang, B. Yu, B.Y. Li, Z.X. Jin, Y.M. Zhao, C. Xue, S.Q. Yu, J.C. Liu, X.F. Wei, Glutaraldehyde and 2,3-butanediol treatment of bovine pericardium for aortic valve bioprosthesis in sheep: a preliminary study, Ann. Transl. Med. 8 (24) (2020).
[84] B. Meuris, S. Ozaki, W. Neethling, S. De Vleeschauwer, E. Verbeken, D. Rhodes, P. Verbrugghe, G. Strange, Trileaflet aortic valve reconstruction with a decellularized pericardial patch in a sheep model, J. Thorac. Cardiovasc. Surg. 152 (4) (2016) 1167–1174.
[85] B. Reichart, D.K.C. Cooper, M. Langin, R.R. Tonjes, R.N. Pierson, E. Wolf, Cardiac xenotransplantation - from concept to clinic, Cardiovasc. Res. 118 (18) (2022) 3499–3516.

Provided by Sächsische Landesbibliothek, Staats- und Universitätsbibliothek Dresden